(NASA CR-54002)
W&S-TR-28

45p

ANALYSIS OF HIGH TEMPERATURE GASES IN SITU BY MEANS OF INFRARED BAND MODELS

by

GUNTER J. PENZIAS AND G. JORDAN MACLAY 15 Dec. 1963 45p

(copy)

PREPARED FOR

NATIONAL AERONAUTICS AND SPACE ADMINISTRATION

(NASA CONTRACT NAS 3-1542, PHASE III)

don't index Phase III

and
THE WARNER & SWASEY COMPANY
CONTROL INSTRUMENT DIVISION
32-16 DOWNING STREET
FLUSHING, NEW YORK 11354

NASA CR-54002
W&S TR-28

FINAL REPORT

ANALYSIS OF HIGH TEMPERATURE GASES IN SITU BY MEANS OF INFRARED BAND MODELS

Gunter J. Penzias and G. Jordan Maclay

Prepared for

NATIONAL AERONAUTICS AND SPACE ADMINISTRATION

December 15, 1963

Contract NAS 3-1542 - Phase III

Technical Management
NASA Lewis Research Center
Chemistry and Energy Conversion Division
E. A. Lezberg

THE WARNER & SWASEY COMPANY
Control Instrument Division
32-16 Downing Street, Flushing, New York 11354

FOREWORD

This report was prepared as part of the task under NASA Contract NAS 3-1542, with NASA Lewis Research Center. Mr. E. A. Lezberg was Technical Manager for NASA.

The authors wish to acknowledge the help of H. J. Babrov, for the many suggestions and criticisms made during the research program, and of R. H. Tourin in preparing this report.

ABSTRACT

A

17598

In order to develop techniques of combustion gas analysis in situ for propulsion research applications, the dependence of infrared absorptance upon partial pressure was investigated for CO_2 and H_2O. The random band model was used to establish quantitative relationships for use in gas analysis. The necessary band model parameters were measured in furnace-heated gases, in flat flames on porous burners, and in shock-heated gases. The variation of these parameters with temperature was measured from 600°K to 2400°K.

Explicit procedures were developed to set up calibration formulae for gas analysis in situ and to determine the parameters needed for applications. Author

TABLE OF CONTENTS

FOREWORD		i
ABSTRACT		ii
LIST OF ILLUSTRATIONS		v
SUMMARY		1
I.	INTRODUCTION	2
II.	METHODS FOR DETERMINING CONCENTRATIONS FROM ABSORPTION MEASUREMENTS	3
	A. Exact Methods	
	B. Approximate Methods	
III.	TECHNIQUES OF FITTING THE STATISTICAL OR RANDOM BAND MODEL	8
IV.	APPARATUS	13
V.	RESULTS	15
	1. Random Model Fit to CO_2 Absorptance Data	
	2. Random Model Fit to H_2O Absorptance Data	
	3. Temperature Dependence of Band Model Parameters for H_2O	
	4. Exact Fundamental Method Applied to H_2O	
VI.	APPLICATION OF ABSORPTANCE MEASUREMENTS TO THE DETERMINATION OF SPECIES CONCENTRATION	22
VII.	CONCLUSIONS	23
REFERENCES		24
DISTRIBUTION		

LIST OF ILLUSTRATIONS

Fig. 1. Shock tube driver section, transition section with valve and pumping station.

2. Warner & Swasey Model 301 High Speed Pyrometer, with covers removed, in place at the shock tube viewing section.

3. Typical oscillographic record of infrared radiance of CO_2 behind the incident shock wave. Modulated (upper) trace represents the spectral absorptance and the unmodulated (lower) trace is a measure of the spectral radiance.

4. CO_2 absorption for several mixture ratios of CO_2 and N_2 at 4.40-μ and 1273°K.

5. CO_2 absorption for several cell lengths at a constant mixture ratio of CO_2 and N_2 at 4.40-μ and 1273°K.

6. Comparison of experimental data and band model prediction for CO_2-N_2 mixtures at 1273°K. The curve is the best fit of the experimental data.

7. Comparison of experimental data and band model temperature interpolation for CO_2-N_2 mixtures at 900°K. The curve is the best fit of the experimental data.

8. Strength band model parameter S^o/d_{CO_2} versus temperature.

9. Ratio of total half-width band model parameter $\frac{\gamma^o}{d}_T$, at temperature T, to half width $\frac{\gamma^o}{d}_{1273}$ at 1273°K versus temperature.

10. H_2O absorption for several mixture ratios of H_2O and N_2 at 2.854-μ and 1273°K for 3.85 cm path length.

11. H_2O absorption for several mixture ratios of H_2O and N_2 at 2.854-μ and 1273°K for a 20.32 cm path length.

12. Comparison of experimental data and band model prediction for H_2O-N_2 mixtures at 1273°K. The curve is the best fit of the experimental data.

Fig. 13. Effect of spectral slitwidth on spectral absorptance and integrated absorptance (equivalent width) for pure H_2O. The lower curve (13a) is a plot of reciprocal transmittance vs the spectrometer slitwidth, for the peak of the spectral transmittance curve at 3504 cm^{-1}. The upper curve (13b) is a plot of equivalent width (area under the spectral transmittance curve divided by I_o) of the same spectral interval. This example illustrates the well known fact that integrated absorptances are independent of spectral resolution.

ANALYSIS OF HIGH TEMPERATURE GASES IN SITU BY MEANS OF INFRARED BAND MODELS

Gunter J. Penzias and G. Jordan Maclay

The Warner & Swasey Company, Control Instrument Division

SUMMARY

In order to develop techniques of combustion gas analysis in situ for propulsion research applications, the dependence of infrared absorptance upon partial pressure was investigated for CO_2 and H_2O. The random band model was used to establish quantitative relationships for use in gas analysis. The necessary band model parameters were measured in furnace-heated gases, in flat flames on porous burners, and in shock-heated gases.

The band model parameters found for CO_2, including the effect of nitrogen-broadening at 4.40-μ and 1273°K, were $(S^\circ/d)_{CO_2} = 3.12\ atm^{-1}cm^{-1}$, $(\gamma^\circ/d)_{CO_2} = 1.667\ atm^{-1}$, $(\gamma^\circ/d)_{N_2} = 0.631\ atm^{-1}$. The variation of these parameters with temperature from 600°K to 2400°K was measured.

The band model parameters for H_2O at 2.854-μ and 1273°K were $(S^\circ/d)_{H_2O} = 0.320\ atm^{-1}cm^{-1}$, $(\gamma^\circ/d)_{H_2O} = 0.444\ atm^{-1}$, $(\gamma^\circ/d)_{N_2} = 0.090\ atm^{-1}$. To predict the temperature variation of the H_2O absorptance, an isolated line model was used which gave good agreement with low temperature measurements. An exact method to determine H_2O concentration was tried which gave fair agreement with experiment. Higher resolution spectral data are necessary to improve the accuracy of this method.

Explicit procedures were developed to set up calibration formulae for gas analysis in situ and to determine the parameters needed for applications.

I. INTRODUCTION

The ability to determine concentrations of chemical species in a hot gas, without the need for removing a sample or disturbing the flow, is desirable for many applications. Techniques to determine concentrations in situ would be helpful in the study of rocket nozzle kinetics, supersonic combustion, and chemical reactions in shock tubes.

We have studied the possible application of infrared combustion gas analysis in situ. The feasibility of the approach was tested first by studying infrared spectra of known gas samples in a special infrared gas cell heated by an electric furnace. By means of the heated gas cell, absorptances of hot carbon dioxide at selected infrared wave lengths were measured at various pressures and temperatures. The gas cell measurements were used to set up a calibration curve, and this curve was applied to determining the CO_2 concentrations in a combustion gas at the same temperature as the gas cell (1). The results were verified independently by gas chromatography analysis.

The demonstration that infrared techniques could be used (1) led to further measurements to determine the effects of path length, total pressure, and pressure of infrared-inactive additive gases on the absorptance of the infrared-active gas (2-4). In the course of this work, it became obvious that a purely empirical approach to setting up calibration curves for infrared analysis in situ would require an impracticably large number of experimental measurements for all possible temperatures, pressures, and mixture ratios. Therefore we next sought to reduce the amount of data required, by making use of the theory of molecular spectra to help establish quantitative relationships between infrared absorptance and concentration at various temperatures and pressures. In particular, we made use of the theory of infrared band models, in which a tractable mathematical representation is used in place of an infrared band consisting of many hundreds or thousands of spectral lines. We first applied band model theory to describe the absorptance of CO_2 at constant temperature (3). Based on the success obtained, efforts were expanded to include the variation of temperature in the band model relationship obtained for CO_2. Similar band model relationships were obtained for water vapor.

This study has been conducted over a range of temperature typical of propulsion research. The lower temperatures (to 1273°K) have been obtained in a quartz sample cell heated within an electric furnace. Intermediate temperatures (1400°K to 1700°K) have been obtained with porous metal (flat flame) burners (5). Higher temperatures

(to 2400°K) have been obtained with a shock tube. The experimental data and the methods employed to determine the band model parameters are discussed in detail in this report. The results of the work leading up to this phase of the research program can be found in references 1, 2, and 3.

II. METHODS FOR DETERMINING CONCENTRATIONS FROM ABSORPTION MEASUREMENTS

A. Exact Methods

A purely empirical approach to determining concentrations is to simply amass absorptance data as a function of temperature, pressure, composition, and geometrical path length at all the anticipated experimental conditions. This method corresponds to a calibration scheme and is exact in that the determination of concentration is as accurate as the calibration measurements. Quite obviously a great many experimental measurements would be required to cover the range of anticipated conditions.

The purely empirical approach to determining concentrations from absorptance measurements is crude in that no use is made of our knowledge of spectroscopy. By judicious application of this knowledge it is possible to considerably reduce the number of experimental measurements required. The general principles of quantitative infrared spectroscopy are well known (6). If a beam of monochromatic infrared radiation is sent through an infrared-active gas, the gas will absorb some of this radiation whenever the frequency of the radiation equals a characteristic vibration frequency of the gas molecule. At such a frequency, the beam emerging from the gas will be weaker than the incident beam, by the amount of energy absorbed. The energy absorbed is, in turn, dependent upon the number of absorbing molecules in the gas path traversed by the infrared beam. The measured strengths of the incident and emergent beams at a frequency ν are related to the absorptance $\alpha(\nu)$ of a line by

$$\alpha(\nu) = 1 - \frac{I}{I_o} \qquad (1)$$

where I_o is the strength of the incident beam, and I is the strength of the transmitted beam. This is the formula used in conventional infrared analysis.

The monochromatic absorptance $\alpha(\nu)$ of a spectral line is given as a function of the frequency by the equation

$$\alpha(\nu) = 1 - e^{-k(\nu)\ell} \quad , \tag{2}$$

where ℓ is the geometrical path length. For a line with a Lorentz line-shape, which is the shape of all infrared absorption lines encountered in practical applications, $k(\nu)$ the absorption coefficient for a line centered at ν_o is given by

$$k(\nu) = \frac{S}{\pi} \frac{\gamma}{(\nu-\nu_o)^2 + \gamma^2} \quad . \tag{3}$$

The absorption coefficient $k(\nu)$ defines a dispersion curve whose half-width at half the maximum value of k is γ. The line parameter γ is therefore called the line half-width. γ is proportional to the number of collisions per second undergone by an absorbing molecule. Each collision is assumed to completely interrupt the radiative process. The half-width is therefore directly proportional to pressure,

$$\gamma = \gamma_a^o P_a + \gamma_b^o P_b \quad , \tag{4}$$

where γ_a^o is the half-width at unit pressure for self-broadening (i.e. for collisions between two absorbing molecules) and P_a is the pressure of absorbing gas. γ_b^o is the half-width at unit pressure for foreign gas broadening (i.e. for collisions between absorbing molecules and other molecules in the gas mixture which do not absorb radiation at frequency ν) and P_b is the pressure of the non-absorbing line-broadening gas.

The parameter S in the absorption coefficient defined by Eq. (3) is called the line strength and is defined by the equation

$$S = \int_o^\infty k(\nu)d\nu \quad , \tag{5}$$

where the line strength is directly proportional to the pressure of the absorbing gas, thus

$$S = S^{o} P_{a} \quad , \tag{6}$$

P_a is the pressure of the absorber, and S^o is the strength at unit pressure.

At a given temperature, each line in the spectrum of an absorbing gas can be completely characterized by two parameters: the line strength S and the line half-width γ. A knowledge of these two parameters and the geometrical path length determines the total or integrated absorptance of an isolated line. The integrated absorptance W of a single isolated line is defined as

$$W = \int_{o}^{\infty} \alpha(\nu) d\nu \quad . \tag{7}$$

Substituting for $\alpha(\nu)$ from Eq. (2), the integrated absorptance can be written as

$$W = \int_{o}^{\infty} (1-e^{-k(\nu)\ell}) d\nu \quad . \tag{8}$$

The integral in Eq. (8) has been evaluated by Ladenburg and Reiche (7) to be

$$W = 2\pi\gamma \, f(x) \quad , \tag{9}$$

where

$$x = \frac{S\ell}{2\pi\gamma} \quad , \tag{10}$$

and f(x) is defined by

$$f(x) = xe^{-x} \left\{ J_o(ix) - iJ_1(ix) \right\} \quad , \tag{11}$$

where $J_0(ix)$ and $J_1(ix)$ are Bessel functions with imaginary arguments.

It would be possible to determine the partial pressure of an infrared-absorbing gas in a mixture from a measurement of the integrated absorptance of a line in a chosen interval, if the center frequencies, strengths, and widths of the lines in the spectral region of interest were known. This could be done at any temperature if the temperature dependence of the strengths and widths of the lines were also known. This procedure may be denoted the exact fundamental method.

One limitation of the exact fundamental method is a lack of knowledge of the strengths and widths of the spectral lines for important gases. Another limitation to this exact method is that for most molecules, and in particular CO_2 and H_2O, the individual lines cannot be isolated with the standard available spectroscopic instrumentation. This can be circumvented for some molecules by measuring the integrated absorptance of all the lines in a chosen interval and subtracting correction terms accounting for the overlapping lines. The end points of the integrated absorptance, however, must go to zero. This condition is met by water vapor for certain spectral intervals in the 2.7-μ band. However, for the 4.3-μ CO_2 band this is not the case, and this exact method could not be applied.

To use this method at various temperatures, the temperature dependence of the strengths and widths must be known. The temperature dependence of the strengths is known accurately. The temperature dependence of the width of the lines, however, is not known accurately and no universally accepted theory about the temperature dependence of the line half-width exists, nor has much experimental research been done on this subject.

B. Approximate Methods

While the exact fundamental approach to relating the infrared absorptance of a gas to its concentration in a mixture requires a great deal of fundamental spectroscopic data which may not always be available, it is useful in establishing relationships. By making some simplifying assumptions, as to variations of the strengths, widths, line spacing, etc. with frequency, temperature, etc. the fundamental relationship can be approximated by some type of mathematically derived scheme (i.e. a band model) which should give results consistent with those calculated by exact methods. Band models are used to relate the average absorptance in a given spectral interval to the concentration

or partial pressure of the absorber and the path length. The band model technique relies on the substitution of an equivalent and mathematically tractable spectrum for the true spectrum in the spectral interval of interest. An example of a band model is the Elsasser (8) model where the assumptions made are constant line spacing, line strength, and line width. In applying the band model technique, use is still made of some fundamental spectroscopic data. These data are referred to as band model parameters. An illustration of a band model calculation is that made by Stull and Plass (9) for HCl which was checked experimentally by Babrov (10).

To avoid unresolved difficulties (missing values of strength, width, etc.) in the calculation of band model parameters, it is possible to employ a semi-empirical approach to the problem of determining these parameters from measurements of the absorptance and a knowledge of the macroscopic coordinates (pressure, path length, temperature). Rather than predict an absorptance from calculated band model parameters and then make a measurement to determine the accuracy of the parameters, it is possible to make the necessary absorption measurements and from the data obtained determine a set of band model parameters. The band model is fitted directly to the absorptance data taken at the same temperature and wavelength at which measurements to determine species concentrations will later be made. This semi-empirical procedure insures that the band model parameters obtained will be of an accuracy dependent only upon the measurement accuracy used to determine these parameters and not upon the validity of any mathematical averaging technique.

A limitation of the empirical band model approach at present is that it does not allow one to extrapolate to temperatures higher or lower than the range of temperatures covered by the experiments performed for the determination of the band model parameters.

One particularly useful band model is the statistical or random band model with random line spacing, constant intensities, and constant widths (11). We have used the statistical band model to correlate water vapor and carbon dioxide absorptance data. The methods used to fit the statistical band model to the absorptance data and obtain the band model parameters are discussed in Section III.

III. TECHNIQUES OF FITTING THE STATISTICAL OR RANDOM BAND MODEL

The band model parameters are obtained directly from absorptance measurements made at a specified temperature and wavelength. Later measurements at this same temperature or wavelength are then used to determine the concentration of a mixture whose composition is not known.

The absorptance of a disordered band (11) is given by

$$\alpha(\nu) = 1 - e^{-W/d} \qquad (12)$$

where $\alpha(\nu)$ is the absorptance and d is the mean line spacing. W is the integrated absorptance of any single line in the band and is given by the Ladenburg-Reiche formula, Eq. (9).

Taking the logarithm of Eq. (12) one obtains

$$\ln (1/\tau) = W/d \quad , \qquad (13)$$

where τ is the transmittance and is equal to I/I_o. Thus the functional relationship between $\ln(1/\tau)$ with cell length and pressure is the same as that for the integrated absorptance.

A frequently employed method of determining S and γ of a single line involved making measurements of the integrated absorptance of an isolated line as a function of the path length. The graph of integrated absorptance vs length in logarithmic co-ordinates is called a curve of growth, and from its asymptotic behavior one can obtain values of S and γ. The statistical model gives the relationship that $\ln(1/\tau)$ is equal to W/d (Eq. (13)) where

$$\frac{W}{d} = 2\pi \frac{\gamma}{d} f\left(\frac{\frac{S}{d} \ell}{2\pi \frac{\gamma}{d}} \right) \quad . \qquad (14)$$

Therefore a band model curve of growth can be used to determine S/d and γ/d. A knowledge of these two parameters permits one to determine the partial pressure (concentration

of absorbing gas) from a measurement of the absorptance and a knowledge of the path length. In case it is found that the experimental data do not determine the usual curve of growth, then either the random model is not applicable to the absorptance data or some function other than f(x) must be used in Eq. (14). The curve of growth method was used recently by Oppenheim and Ben-Aryeh (12) for the 4.3-μ region of the CO_2 spectrum, at 1200°K.

In this laboratory, another technique has been used for fitting the random model to absorptance data. Our experiments include broadening by nitrogen and other gases in addition to the self-broadening by the absorber. If γ_a^o/d and γ_b^o/d are respectively the self-broadened half-width and the foreign gas broadened half-width, both at one atmosphere pressure, then in a given experiment the combined half-width is given by Eq. (4). Equation (4) can be rewritten, if the substitution is made that the mixture ratio, m, equals P_b/P_a. Equation (4) then reduces to

$$\frac{\gamma}{d} = P_a \left[\frac{\gamma_a^o}{d} + m \frac{\gamma_b^o}{d} \right] \quad . \tag{15}$$

The expression for the logarithm of the reciprocal transmittance can therefore be rewritten

$$\ln \left(\frac{1}{\tau}\right) = 2\pi P_a \left[\frac{\gamma_a^o}{d} + m \frac{\gamma_b^o}{d} \right] f(x) \quad , \tag{16}$$

where

$$x = \frac{\frac{S^o}{d} \ell}{2\pi \left(\frac{\gamma_a^o}{d} + m \frac{\gamma_b^o}{d} \right)} \quad . \tag{17}$$

Note that x is independent of pressure if the mixture ratio m is held constant.

Equation (16) can be rewritten

$$\frac{\ln\left(\frac{1}{\tau}\right)}{P_a} = C\left(\frac{S^o}{d}, \frac{\gamma_a^o}{d}, \frac{\gamma_b^o}{d}, m, \ell\right) \quad , \qquad (18)$$

Where C, constant with pressure, is the slope of a straight line representing the graph $\ln(1/\tau)$ vs P_a. To fit the random model to our experimental data, the parameters S^o/d, γ_a^o/d, and γ_b^o/d must be determined. Since there are three unknowns, absorptance measurements at three different mixture ratios and/or cell lengths must be made.

The equations to be solved are as follows:

$$C_1 = 2\pi \frac{\gamma_1}{d} f\left(\frac{S^o/d\ \ell_1}{2\pi \frac{\gamma_1}{d}}\right) \qquad (19a)$$

$$C_2 = 2\pi \frac{\gamma_2}{d} f\left(\frac{S^o/d\ \ell_2}{2\pi \frac{\gamma_2}{d}}\right) \qquad (19b)$$

$$C_3 = 2\pi \frac{\gamma_3}{d} f\left(\frac{S^o/d\ \ell_3}{2\pi \frac{\gamma_3}{d}}\right) \quad , \qquad (19c)$$

where

$$C = \frac{\ln\left(\frac{1}{\tau}\right)}{P_a}$$

and

$$\frac{\gamma_1}{d} = \frac{\gamma_a^o}{d} + m_1 \frac{\gamma_b^o}{d}$$

$$\frac{\gamma_2}{d} = \frac{\gamma_a^o}{d} + m_2 \frac{\gamma_b^o}{d}$$

$$\frac{\gamma_3}{d} = \frac{\gamma_a^o}{d} + m_3 \frac{\gamma_b^o}{d} \quad .$$

The subscripts 1, 2, and 3 refer to the three different mixture ratios. All these measurements, however, are made at the same wavelength and temperature. An iterative method for solution of these equations has been described in detail by Babrov (13).

In principle, one could fit the absorptance data to the band model if only three measurements were made. The accuracy of the values obtained, however, depends on the sensitivity of the particular experiments conducted. In practice the following experimental conditions are used to obtain maximum accuracy. One experiment must be conducted on pure absorber. For this experiment the value of x should be high. The other two experiments are on mixtures of absorber and broadener: one of the measurements should have as low an x as possible, and the other experiment a very high x. The low x data may be obtained with a short path length and a large mixture ratio. The high x data may be obtained with a large path length and a mixture ratio small relative to that used in the low x experiment. The greater the ratio of high x to low x, the greater the accuracy of the value determined for S^o/d. The accuracy is also improved if the ratio of the path length in the two experiments is as great as possible. This difference in path length is desirable because one cannot achieve optimum accuracy by manipulation of mixture ratio alone. The mixture ratio in the high x measurement must not be too small, since it affects the accuracy of the value found for γ_b^o/d. The relationship between the relative error $\ln(1/\tau)$ and the relative error in γ_b^o/d is given by

$$\frac{\Delta\left(\frac{\gamma_b^o}{d}\right)}{\frac{\gamma_b^o}{d}} = \phi_m \frac{\Delta\,(\ln 1/\tau)}{\ln 1/\tau} \quad , \qquad (20)$$

where

$$\phi_m = \left(1 + \frac{\gamma_a^o}{\gamma_b^o}\,\frac{1}{m}\right)\left(\frac{f(x)}{f(x)-xf'(x)}\right) \quad . \quad (21)$$

It can be seen from Eq. (21) that as m goes to zero the error in γ_b^o increases rapidly. Therefore to avoid large errors in the determination of γ_b^o/d, the mixture ratio used to determine γ_b^o/d should be chosen so that the total half-width is due to a significant extent to the foreign gas broadening.

The value of γ_a^o/d is determined from the self-broadened experiment, i.e. the experiment with the pure absorber. In this experiment, x is high and Eq. (16) can be approximated by

$$\ln\frac{1}{\tau} = 2\,P_a\left(\frac{S^o}{d}\,\frac{\gamma_a^o}{d}\,\ell\right)^{\frac{1}{2}} \quad . \quad (22)$$

Therefore the relative error in the line width is twice the relative error in $\ln(1/\tau)$.

In summary, if only three measurements are to be made, then to obtain optimum accuracy the following experiments should be performed: (1) Short path, large pressure of broadener relative to the pressure of absorber; (2) long path and moderate pressure of broadener relative to pressure of absorber; (3) long path and pure absorber. The accuracy of the determination of the band model parameters is improved if more than three measurements are made. Since $\ln(1/\tau)$ varies linearly with pressure at a constant mixture ratio, by plotting the results of a series of measurements of $\ln(1/\tau)$ at different pressures for a constant mixture ratio, the value of C can be accurately determined from the slope of the line. Clearly, it is undesirable to measure absorptances near unity or zero for input to the random band model because the error in determining $\ln(1/\tau)$ becomes extremely large. The techniques mentioned above have been used to obtain band model parameters for CO_2 and H_2O and are described in Section V below.

The above discussion pertains to absorption measurements made at one temperature. To obtain the temperature variation of absorptance as a function of path length, pressure and concentration, it is necessary to

perform a series of measurements as described above at various temperatures and obtain the band model parameters. The parameters can then be graphed as a function of temperature, for interpolation.

IV. APPARATUS

The absorptances of hot CO_2 and H_2O were obtained from measurements in furnace-heated gas cells, flames, and shock-heated gases. The experimental setup used to measure the infrared absorptance of CO_2 and H_2O in gas cells has been previously described (1-3). For the water vapor measurements, the flushed gas cell spectrometer system was modified by replacing the Littrow mirror in the monochromator with a diffraction grating. This improved the resolution of the instrument. A lead sulfide detector was also used in place of the ordinary vacuum thermocouple. This enabled narrower slits to be used while still maintaining a good signal-to-noise ratio.

To obtain measurements at higher temperatures than possible with the electric furnace, a shock tube system was used. The driven (low pressure) section consisted of several lengths of 304 stainless steel seamless tubing having $2\frac{1}{4}$" i.d. and sections flanged at both ends. When completely assembled the low pressure section was 15 feet in length, with the point of observation located $13\frac{1}{2}$ feet from the diaphragm. The driver (high pressure) section was constructed of stainless steel with an overall length of 4 feet having a 4 inch i.d. To connect the driver to the driven section, a smooth converging transition section was used. A 2-inch valve was incorporated into this transition section to permit rapid evacuation of the shock tube. Figure 1 shows the driver section and the large 2" diameter valve in the converging section connected to a 2-inch diffusion pumping station backed by a Welch Duo-Seal Pump. The diaphragm was located at the upstream side of the transition section (i.e. across the 4-inch diameter), which enhances the shock tube operation (14). The diaphragm holder is shown open in Fig. 1. A typical ruptured aluminum diaphragm is visible on top of the pumping station in Fig. 1. Aluminum and Mylar diaphragms were used. Both diaphragms were ruptured by increasing the pressure in the driver section. In all cases, the opening was found to be satisfactory as evidenced by the petal formation of the ruptured diaphragms.

The shock velocity was measured by using thin film resistance probes (14,15). Two probes located 200 mm and 822 mm before the observation point were used to determine

the velocity. The probe output triggered a Thyratron circuit, and the resultant pulse was then displayed on an oscilloscope modified for a raster sweep display (16). A time mark generator was used to time the raster sweep, resulting in a time measurement accurate to better than 1 microsecond and a resultant error in the velocity measurement of less than ½%.

The absorptance and temperature of the shock-heated CO_2 were measured using a Warner & Swasey Model 301 High Speed Pyrometer, which consists of a source unit and a receiver-monochromator unit. The instrument was located 13½ feet from the diaphragm, at the viewing section, which contained two 1/8-inch thick sapphire windows mounted in line. The source unit, shown on the left in Fig. 2, is placed on one side of the shock tube and contains a globar, Cassegrainian optics, and a high speed air turbine chopper. The source unit generates a beam of radiant energy modulated at 90,000 to 180,000 cycles per second, directed through the viewing windows in the shock tube, to the receiver-monochromator unit. When the shock passes the windows, the heated gases absorb some of this modulated radiation. This reduction of intensity is a measure of the gas absorptance.

The modulated radiation beam from the source unit and the radiant energy produced by the shock-heated gases are collected by the receiver-monochromator unit, shown on the right in Fig. 2, which is located on the other side of the shock tube from the source unit. The receiver unit contains Cassegrainian optics to collect the energy and focus it at the entrance slits of the grating monochromator. The collected energy passes through the monochromator, which is set at a particular wavelength. The radiant energy within the infrared band passed by the monochromator is focused on an indium antimonide liquid-nitrogen-cooled infrared detector. The time constant of the detector is less than one microsecond. The detector output is amplified and displayed on a dual-beam oscilloscope. A typical record is shown in Fig. 3. The upper modulated trace is a measure of the gas absorptance, and the lower trace is a measure of the spectral radiance, both at the selected wavelength. A standard strip lamp is incorporated in the receiver unit; it is used to calibrate the spectral radiance in absolute units. It is then possible to determine the gas temperature (17) as well as the absorptance. The data reduction method and the principle involved in determining the temperature are described in great detail in reference 16.

The CO_2-nitrogen mixtures were prepared by the method of partial pressures in a mixing chamber (16) and were allowed to stand for twenty-four hours before use. The shock tube was evacuated to a pressure of a few microns

before filling, and the shock tube system had an overall leak rate of less than 1 micron per minute. Initial pressures varied from 11 to 15 mm Hg abs for the CO_2-nitrogen mixtures and 2 mm Hg abs for pure CO_2. The available testing time was greater than 150 microseconds, which was more than adequate, in view of the microsecond response time of the instrumentation. The initial pressures in the low pressure section were measured by using a double reduction technique (13) which permitted the initial pressure to be measured to .02 mm Hg abs.

V. RESULTS

1. Random Model Fit to CO_2 Absorptance Data

Using the techniques described in Section III, the random band model was fitted to CO_2 absorptance measurements at 4.40-μ and 1273°K. Some of the experimental data are shown in Figs. 4 and 5. Additional results have been previously reported (1-3). The specific experimental conditions are given in Table I.

Table I. Fitting the random band model to CO_2 absorptance measurements. The symbols are defined in Eqs. (4), (10), (13).

Parameter	Experiment		
	High x	Low x	Self-broadening
Cell length ℓ cm	12.7	3.85	7.62
Mixture ratio $m = P_b/P_a$	3.18	33.13	0
$C = \frac{\ln(1/\tau)}{P_a}$	21.92	11.52	11.81

The band model parameters were calculated from the experimental data in Table I by means of Eq. (19). The results are as follows:

$$S^{o}/d = 3.12 \text{ atm}^{-1}\text{-cm}^{-1} ,$$

$$\gamma^{o}/d \; CO_2 = 1.667 \text{ atm}^{-1} ,$$

$$\gamma^{o}/d \; N_2 = 0.631 \text{ atm}^{-1} .$$

Using these parameters, the partial pressure of CO_2 in an unknown mixture can be determined from low resolution absorptance measurements ($\Delta\nu$ = 5 to 40 cm^{-1}) at 4.40μ and 1273°K, for known geometrical path length ℓ and total pressure.

To determine the accuracy of the band model fit, the random model was used to predict CO_2 at 4.40μ and 1273°K, as a function of absorber pressure and cell length, at constant total pressure. The predicted absorptances were compared to measured values, with the result shown in Fig. 6. The agreement between experimental and calculated absorptance is within 3 percent over the entire range of conditions. The small dependence of absorptance on cell length shown by the calculations is too small to be detected experimentally.

In addition to 1273°K, measurements were also made in the furnace-heated gas cell system at 600°K and 900°K. For these two temperatures, the experimental data were also fitted to the random band model, and the agreement between experimental measurements and calculated absorptances was excellent. Results for 900°K are shown in Fig. 7.

To obtain CO_2 absorptance data at temperatures above 1273°K, measurements were made with the shock tube system, for several mixture ratios and pressures, at 2040°K and 2330°K. The temperatures and pressures were calculated from the measured shock velocity. Using the method suggested by Gaydon (14), we assumed a chemically frozen and vibrationally equilibrated state behind the incident shock. This is a valid asumption, since the CO_2 decomposition is relatively slow (22). The emission and absorption records were constant with time during the measurement, as shown in Fig. 4, further substantiating the assumption. The absorption data were obtained 70 microseconds (laboratory time) behind the incident shock. The gas temperatures were measured by an infrared emission-absorption method (17) and the agreement with the theoretical calculations was within the experimental error of 5%.

From the shock tube measurements it was possible to determine the band model strength parameter S^o/d. Additional experimental absorptance data obtained from the literature (15,18) for temperatures between 1400 and 2400°K were also used. The strength parameter is plotted as a function of temperature in Fig. 8. Similar data for the half-width parameter are shown in Fig. 9, where the ratio of the half-width parameter at temperature T to its value at 1273°K is plotted vs temperature. Note that the half-width parameter increases with temperature, although in general one expects the half-width of a single line to decrease with increasing temperature. This apparently anomalous behavior of the CO_2 half-width parameter is due to the increasing number of hot bands and the resulting decrease in the mean line spacing. The half-width of the line may be decreasing with increasing temperature, but the mean line spacing is decreasing more rapidly. Most of the high temperature measurements were made at low values of x, and consequently it was not possible to precisely determine the half-width parameter as a function of temperature above 1273°K. The error in S^o/d introduced by the half-width temperature extrapolation shown in Fig. 9 is less than 10%.

The results of the band model fit with temperature represented by Figs. 8 and 9 constitute the first attempt to account for the effect of temperature on absorptance using the empirical band model approach. Due to the limited experimental data currently available at temperatures above 1273°K, the accuracy of the strengths and half-widths is on the order of 10%, while below 1273°K the accuracy of the parameters is better than 3%. To improve upon the accuracies of these curves, additional measurements are required with the shock tube system and flat flame burners. The use of the flat flame burner was limited by the burner diameter and mixture ratio available for stable burning. This situation has recently been improved with the construction of several rectangular burners in our laboratory. By placing several burners in series it will be possible to vary the path length. To obtain a greater variance in the concentration of CO_2, it has been suggested (19) that combustible gas mixtures of hydrogen, carbon monoxide, and air or oxygen be prepared to give the desired partial pressures of CO_2. The combination of several burners and a tailored combustible gas mixture can be used to obtain more data to improve the accuracy of the strength and half-width curves.

It is possible to account for the presence of other broadening gases, using relative (to nitrogen) broadening, since the effect of nitrogen broadening was determined in the statistical model relationships. The broadening effects of oxygen, water vapor, and helium on CO_2 absorptance, relative to nitrogen, have been previously determined (2,3). To include all the major products of combustion, measurements with CO as broadening gas remain to be made.

2. Random Model Fit to H_2O Absorptance

Using the band model fitting technique previously described, water vapor absorptances measured at 2.854-μ and 1273°K were used to obtain the band model parameters. The measurements were made in the furnace-heated gas cells. The absorptance, expressed as $\ln(1/\tau)$, was plotted against absorber pressure for different mixture ratios and different length cells, as shown in Figs. 10 and 11. The curves in Figs. 10 and 11 are straight lines through the origin, confirming that the data can be correlated to the random model. The band model parameters obtained from the data at 2.854-μ at 1273°K, with a spectral slit of 2 cm^{-1}, are as follows:

$$S^o/d = 0.320 \text{ atm}^{-1}\text{cm}^{-1}$$

$$\gamma^o/d \; H_2O = 0.444 \text{ atm}^{-1}$$

$$\gamma^o/d \; N_2 = 0.090 \text{ atm}^{-1}$$

A comparison of the band model parameters and experimentally measured absorptances was made for water vapor-nitrogen mixtures at constant total pressures in cells of different lengths. The results are shown in Fig. 12, where the absorptance has been plotted as a function of optical depth ($P_a \ell$). The agreement is quite good.

The wavelength 2.854-μ was chosen because of the strongly absorbing water vapor lines at this frequency. The relatively high absorptance reduced the experimental error for low water vapor concentration measurements. However, at this frequency CO_2 also has an absorption band. Therefore, when CO_2 is present in the combustion gas stream, measurements must be made at some other wavelength where the CO_2 does not interfere, in order to determine the H_2O concentration. Such a wavelength is 2.506-μ. Sufficient data were obtained at 2.506-μ, so that the band model parameters could also be determined at this wavelength. (Time requirements did not permit determination of the parameters at 2.506-μ). The accuracy of the measurements at 2.506-μ is somewhat less than for the measurements at 2.854-μ, due to the somewhat lower absorptance of water vapor at 2.506-μ.

Both H_2O frequencies were chosen away from the band center, where the absorption is highest, because the optical path must be flushed to eliminate interference by atmospheric water. It was found that, while it was not possible to eliminate all of the atmospheric water vapor

absorption, it was possible to remove a sufficient amount of water vapor so that no interference was obtained at either of the two frequencies used.

At the present time there is an insufficient number of experimental water vapor absorptance data at temperatures above 1273°K for use in obtaining the band model parameters for water. The flat flame burner measurements made in this laboratory were limited to a narrow range of optical depth. With the construction of several rectangular burners, and using a tailored combustible gas mixture, it is hoped that the proper type of absorptance data can be obtained with the burners. Use can also be made of the shock tube system to obtain absorptance data at higher temperatures.

3. Temperature Dependence of Band Model Parameters for H_2O

A semi-theoretical single-line approach was used to predict the temperature dependence of the basic band model parameters, S°/d and γ°/d. This procedure can be justified on the grounds that the lines within the spectral slitwidth at 600°K can be considered to be the lines within the spectral slitwidth at 1273°K. This is due to the fact that at 1273°K only one or two hot bands of the 2.7-μ, ν_3 fundamental band of H_2O absorb significantly. In this analysis, the band model strength parameter has been assumed to vary with temperature in the same way that the strength of a single isolated water vapor line varies with temperature (20). Thus

$$\frac{S^\circ(T)}{d} = \frac{S^\circ(1273)}{d} \left\{ \exp\left[-2160 \left(\frac{1}{T} - \frac{1}{1273} \right) \right] \right\} \left(\frac{1273}{T} \right)^{5/2} . \quad (23)$$

In addition, it is assumed that the temperature variation of the total half-width (self-broadened plus foreign gas-broadened) is given by

$$\frac{(\gamma^\circ/d)\ 1273}{(\gamma^\circ/d)\ T} = \left(\frac{T}{1273} \right)^n , \quad (24)$$

where $n = 0.6$ from $600^\circ K < T < 1200^\circ K$

$n = 0.66$ from $1200^\circ K < T < 2400^\circ K$.

These values of n are average values obtained by Benedict and Kaplan (21). Using the temperature relationships given by Eqs. (23) and (24), the absorptance of water vapor at 637°K at 2.854-μ was calculated and then compared to experimental measurements made in the gas cells. The results are shown in Table II.

Table II

P_{H_2O} mm Hg	P_{N_2} mm Hg	ℓ cm	Measured $\alpha(\nu)$	Predicted $\alpha(\nu)$
150	---	20.32	0.560	0.542
125	312	20.32	0.555	0.537

The agreement is good. The agreement with experimental measurements made with the flat flame burner for H_2-air flames at temperatures between 1300°K and 1650°K was poor. The poor correlation may be due to experimental error or to some error in the temperature relationship given in Eqs. (23) and (24). The lack of agreement indicates more work is required at higher temperatures.

4. Exact Fundamental Method Applied to Water Vapor

In using the band model parameters for water vapor, it is necessary to specify the spectral slitwidth. This is extremely important for the water absorptance measurements, since the absorptance varies with spectral resolution. This variation is shown in Fig.13a, where $\ln(1/\tau)$ has been plotted against mechanical slitwidth (which is directly proportional to the spectral slitwidth). In order to use the band model parameters in practice it will be necessary to adjust the spectral slitwidth of the measuring instrument to be the same as that used to obtain the band model parameter fit. Although it is possible to do this in practice, it does impose a condition upon the use of the band model parameters. To avoid this difficulty, a different approach to the determination of concentrations was attempted, which makes use of the integrated absorptance, defined by Eq. (8), rather than the fractional transmittance. It is known that the integrated absorptance is insensitive to a change in spectral resolution as long as the absorptance is zero at the end points of the integration. For the

spectral lines considered in the water vapor measurements, around 2.854-μ and 2.506-μ, this was not quite the case; nevertheless, the change in integrated absorptance as a function of spectral slitwidth was very small, as shown in Fig. 13b. Since the use of integrated absorptance is adapted to the exact fundamental method previously discussed, an attempt was made to fit the two groups of lines in the 2.7-μ band using the calculation. There are approximately 12 lines in the 3499.7 – 3504.7 cm^{-1} group, and 11 lines near 3989.5 – 3991.6 cm^{-1}. The basic theoretical formulae used in the predictions permit variation of geometrical path length, water vapor pressure, temperature, and pressure of broadener. Since neither the strengths nor widths of the lines in the interval chosen had been measured previously, they were calculated. In addition, Benedict and Kaplan's (21) calculations, based on the Anderson theory of pressure broadening, were used to obtain the half-widths. The line strength calculations required a knowledge of two parameters, both of which were unknown. One parameter was the band strength S_ν of the ν_3 fundamental band, i.e. the sum of the strengths of all the lines in the band; the other parameter was β, which is used to account for effects coming from the interactions of vibration and rotation of the molecules. The values of S_ν and β were determined from our measurements such that the calculated intergrated absorptances agreed most closely with the measured integrated absorptances. The best agreement was obtained when β was approximately equal to 0.04 and S_ν was equal to 195 cm^{-1}/atm-cm at 300°K.

The agreement between calculated and experimental integrated absorptances was within 10%, which is not sufficiently accurate for a concentration determination. The discrepancy is due to the uncertainties of the basic line parameters used in the calculations. To measure the line parameters, a spectral resolution of the order of 0.1 cm^{-1} is necessary to resolve the water vapor lines in the spectral interval being considered. Therefore, in order to use the fundamental approach to predicting the integrated absorptance of water vapor, measurements of the basic line parameters will have to be made using high resolution. A high resolution spectrometer has been constructed in our laboratory and will be available shortly for these fundamental measurements. With the basic line parameters, the use of this exact fundamental method should be more fruitful.

VI. APPLICATION OF ABSORPTANCE MEASUREMENTS TO THE DETERMINATION OF SPECIES CONCENTRATIONS

With the fitting of the CO_2 and H_2O absorptance data to the random band model, it is now possible to determine species concentrations from measured absorptances without amassing absorptance data at all anticipated experimental conditions. The following step-by-step procedures can be applied in determining the concentrations:

(1) Determine the geometrical path length ℓ in cm.

(2) Determine the total pressure and the temperature of the phenomenon being investigated.

(3) Measure the absorptance of the species to be determined, at the specified frequency and spectral slit-width of the band model parameters to be used. It is possible to simultaneously measure the gas temperature by the infrared emission-absorption method (16,17).

(4) From a knowledge of the gas temperature, the values of S^o/d and γ^o/d are determined from graphs similar to Figs. 8 and 9.

(5) Using the information obtained in steps (1) through (4), the following equations are solved for P_a, the pressure of the absorbing gas in atmospheres, which is the desired result.

$$\ln \frac{1}{\tau} = \frac{(S^o/d)P_a \ell f(x)}{x} \tag{25}$$

$$x = \frac{(S^o/d)\ P_a \ell}{2\pi \left[P_a \frac{\gamma_a^o}{d} + (P_T - P_a) \frac{\gamma_b^o}{d}\right]} \tag{26}$$

The solution to the above equations requires trial and error; however the number of trials may be reduced by a judicious first choice of P_a, based upon the theoretical concentrations expected for the gas phenomenon. Equations (25) and (26) can be solved graphically at a given temperature. The absorptance, which is related to $\ln(1/\tau)$ can be plotted against optical depth, $P_a\ell$, at a constant pressure. The resulting graph would be similar to Fig. 6. Such a graph would be useful for repeated application

to the determination of the concentration at one temperature. If a narrow range of temperatures and pressures are to be considered, then a series of such graphs might be desirable as a substitute for the analytical solution to the above equations.

VII. CONCLUSIONS

CO_2 absorptance data have been fitted to the random band model, and the effect of nitrogen gas broadening has been determined. The band model parameters have been determined as a function of temperature from 600°K to 2400°K. The effects of the relative broadening ability of oxygen and water vapor on CO_2 have previously been determined. The effect of carbon monoxide broadening must still be determined. The accuracy of the band model parameters at temperatures higher than 1273°K must be improved by obtaining these parameters from more experiments.

The random band model has been used to fit the water vapor absorptance data at 1273°K, including the effect of nitrogen foreign gas broadening. Initial attempts at determining the variation of absorptance with temperature were partially successful. More experiments at higher temperatures are required. This can be accomplished with shock tube and burner measurements. In addition, the effect of foreign gas broadening must be checked experimentally for inert gases other than N_2, in particular CO, CO_2, and O_2.

To improve the fundamental approach using the integrated absorptance, high resolution measurements (0.1 cm^{-1}) are required. These measurements can be made using a high resolution spectrometer.

REFERENCES

1. G. J. Penzias and R. H. Tourin, Combustion and Flame 6, 147 (1962).

2. G. J. Penzias, H. J. Babrov, and R. H. Tourin, Final Report on Phase I of Contract NAS 3-1542 (1961).

3. G. J. Penzias, G. J. Maclay, and H. J. Babrov, NASA CR 1, Final Report on Phase II of Contract NAS 3-1542 (1962).

4. R. H. Tourin and H. J. Babrov, J. Chem. Phys. 37, 581 (1962).

5. W. E. Kaskan, Sixth Symposium on Combustion (Reinhold Publishing Corp., New York, 1957), p. 34.

6. G. R. Harrison, R. C. Lord, and J. R. Loofbourow, Practical Spectroscopy (Prentice-Hall, New York, 1948), Ch. 14 and 17.

7. R. Ladenburg and F. Reiche, Ann. Phys. 42, 181 (1911).

8. W. M. Elsasser, Heat Transfer by Infrared Radiation in the Atmosphere (Harvard Meteorological Studies No. 6, 1942).

9. V. R. Stull and G. N. Plass, J. Opt. Soc. Am. 50, 1279 (1960).

10. H. J. Babrov, J. Opt. Soc. Am. 53, 945 (1963).

11. G. N. Plass, J. Opt. Soc. Am. 48, 690 (1958).

12. U. P. Oppenheim and Y. Ben-Aryeh, J. Opt. Soc. Am. 53, 344 (1963).

13. H. J. Babrov, G. Ameer, and W. Benesch, AFOSR TR-59-207, Final Report under Contract AF18(600)-986, University of Pittsburgh (1959).

14. A. G. Gaydon and I. R. Hurle, The Shock Tube in High-Temperature Chemical Physics (Reinhold Publishing Corp., New York, 1962).

15. M. Steinberg and W. O. Davies, J. Chem. Phys. 34, 1373 (1961).

16. G. J. Penzias and R. H. Tourin, Technical Report on Contract AF33(616)-8319, ARL 63-85 (1963), Wright-Patterson Air Force Base, Ohio.

17. R. H. Tourin, Temperature, Its Measurement and Control in Science and Industry, Vol. III, C. M. Herzfeld, Ed. (Reinhold Publishing Corp., New York, 1962), Part 2, Ch. 43.

18. C. C. Ferriso, J. Chem. Phys. 37, 1955 (1962).

19. F. Belles, private communication, 1963.

20. W. S. Benedict, R. Herman, G. E. Moore, and S. Silverman, Can. J. Phys. 34, 830 (1956).

21. W. S. Benedict and L. D. Kaplan, J. Chem. Phys. 30, 388 (1959).

22. T. A. Brabbs, F. E. Belles, and S. A. Zlatarich, J. Chem. Phys. 38, 1939 (1963).

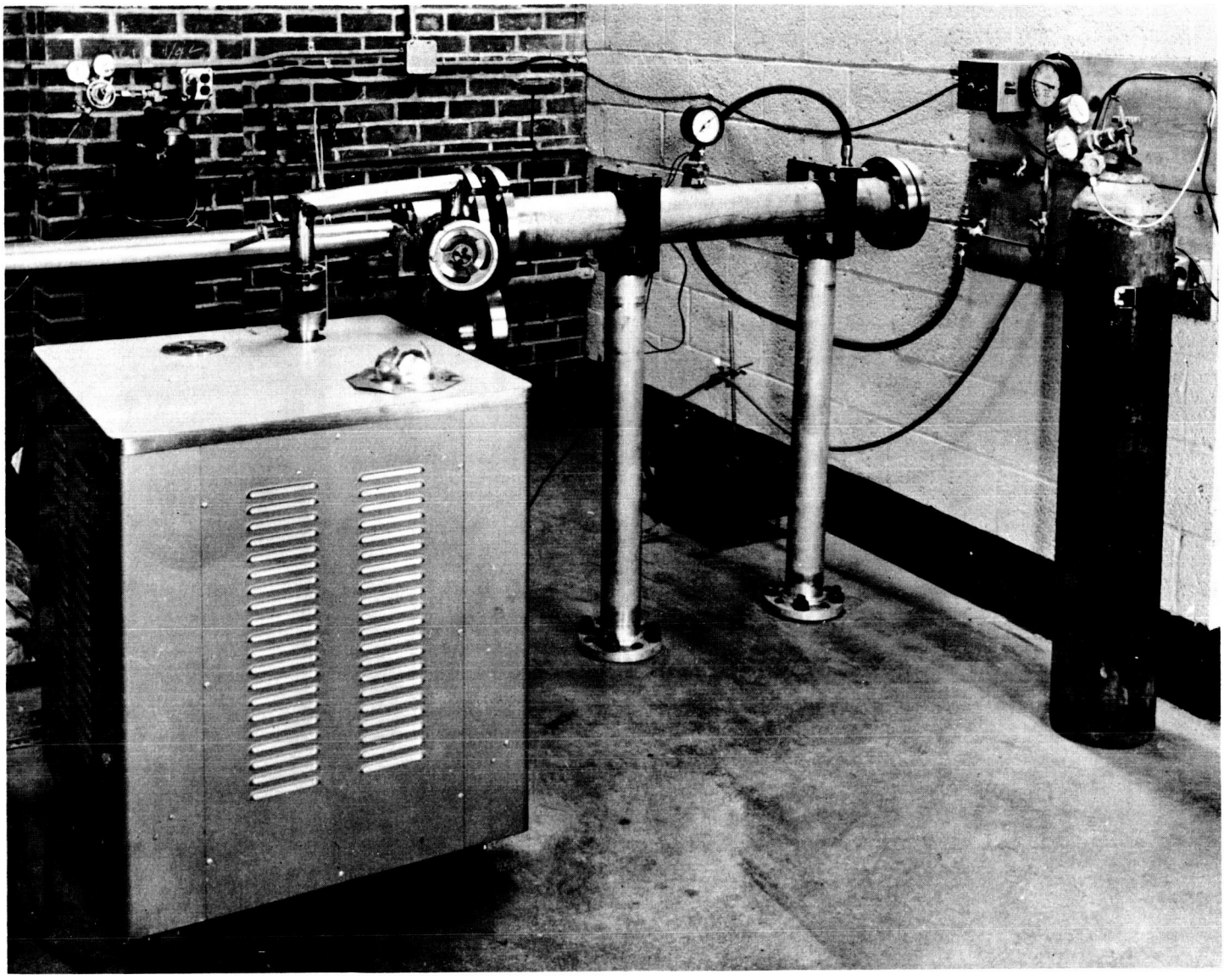

Fig. 1. Shock tube driver section, transition section with valve and pumping station.

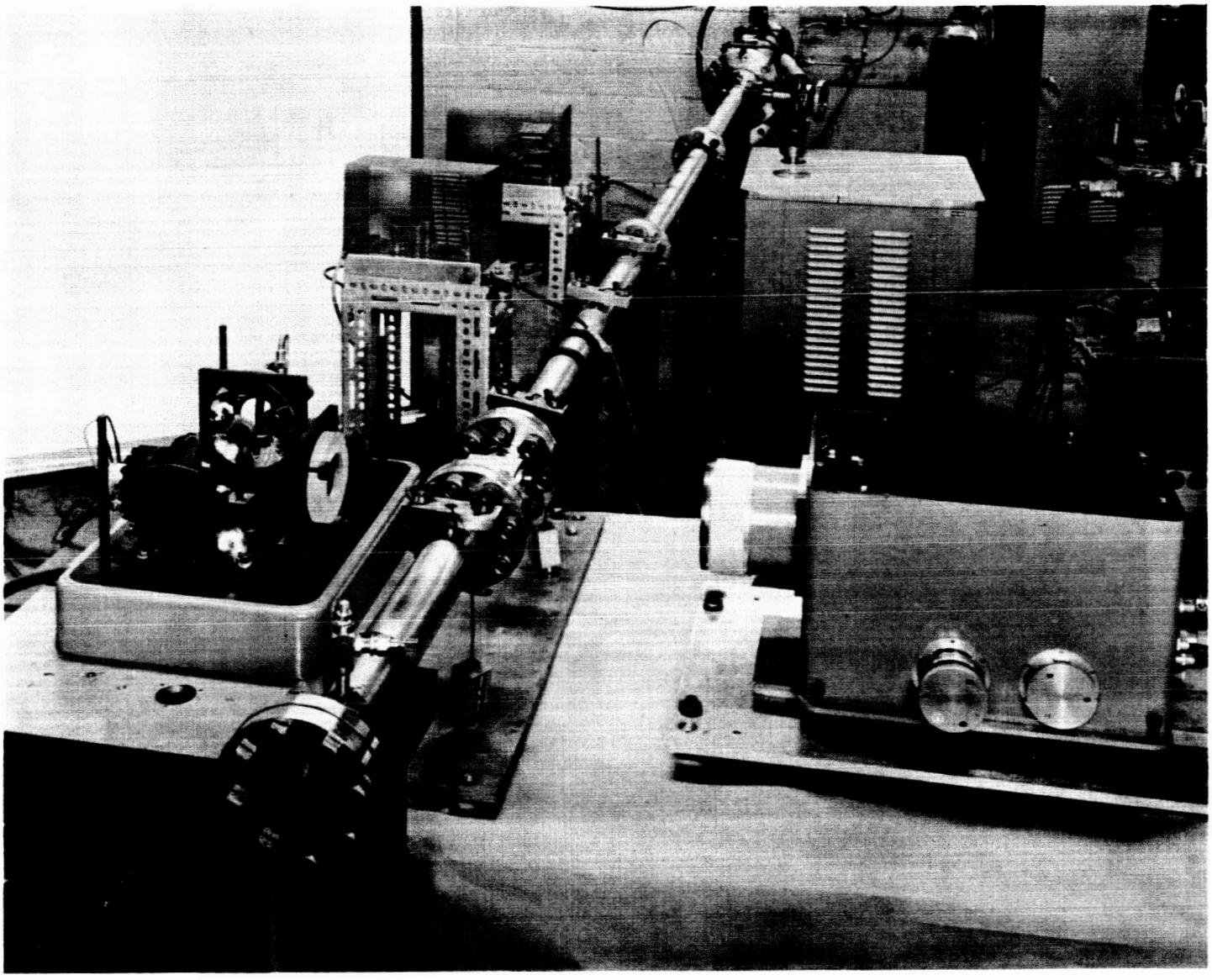

Fig. 2. Warner & Swasey Model 301 High Speed Pyrometer, with covers removed, in place at the shock tube viewing section.

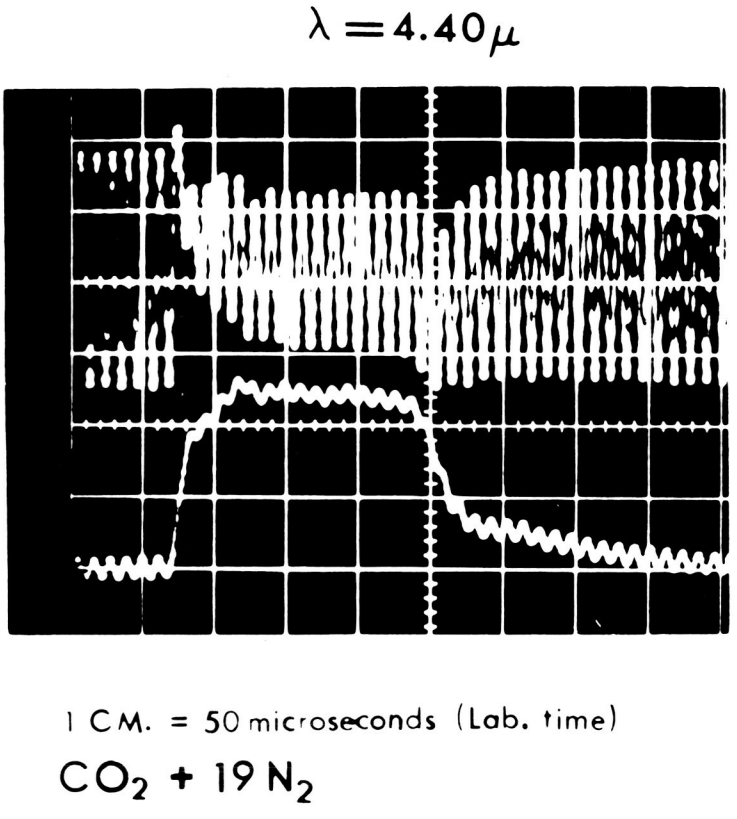

Fig. 3. Typical oscillographic record of infrared radiation of CO_2 behind the incident shock wave. Modulated (upper) trace represents the spectral absorptance and the unmodulated (lower) trace is a measure of the spectral radiance.

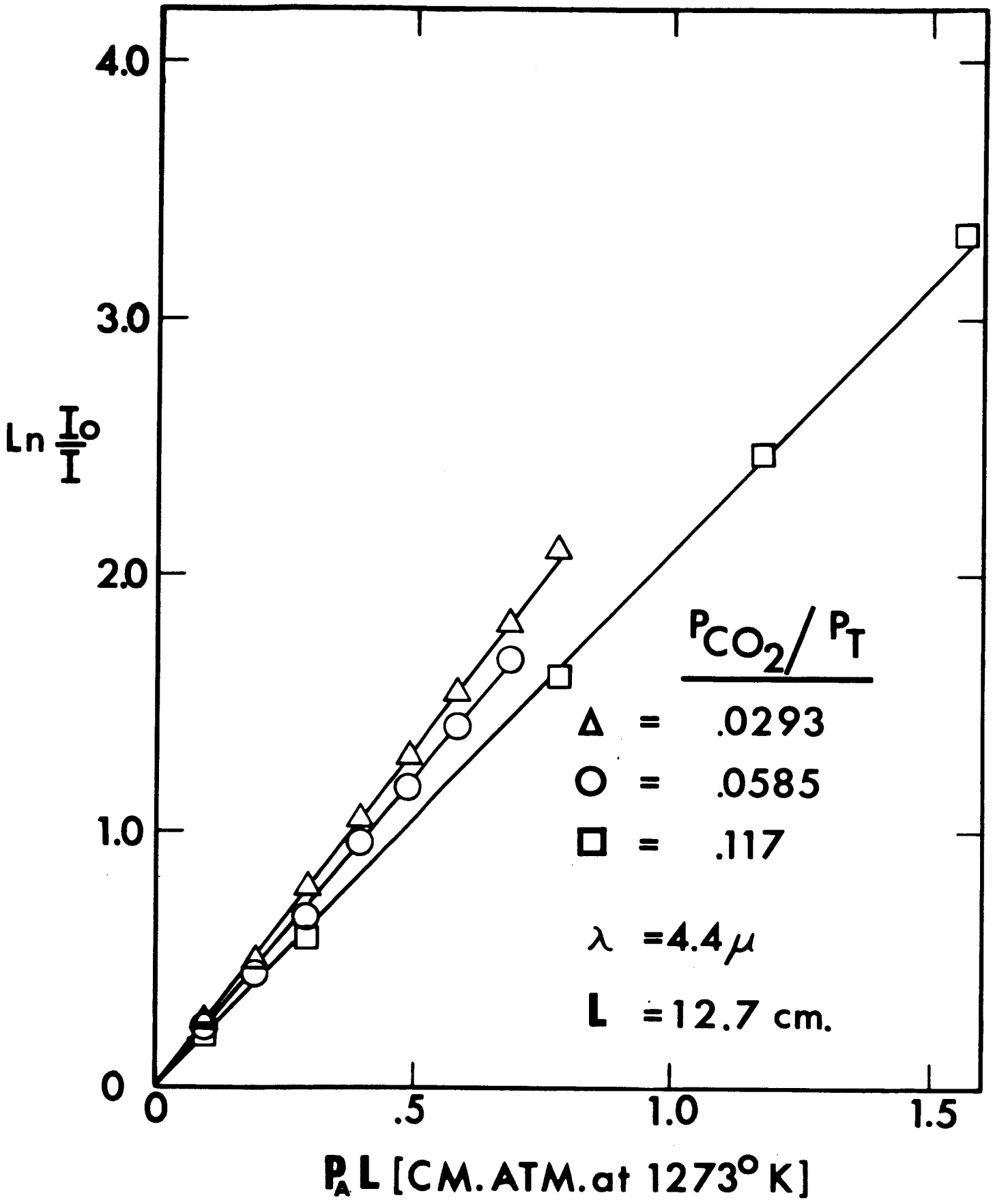

Fig. 4. CO_2 absorption for several mixture ratios of CO_2 and N_2 at 4.40-μ and 1273°K.

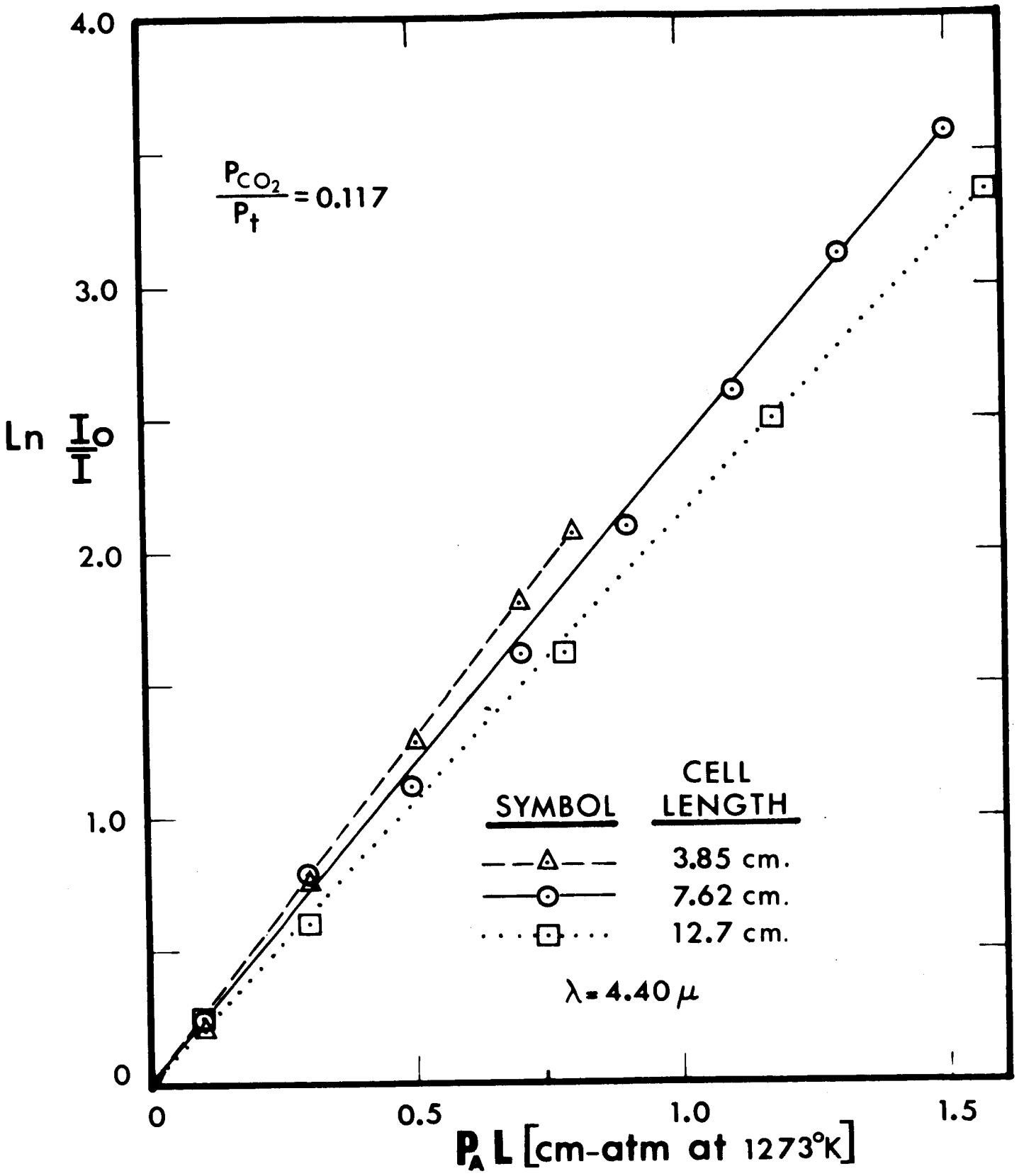

Fig. 5. CO_2 absorption for several cell lengths at a constant mixture ratio of CO_2 and N_2 at 4.40-μ and 1273°K.

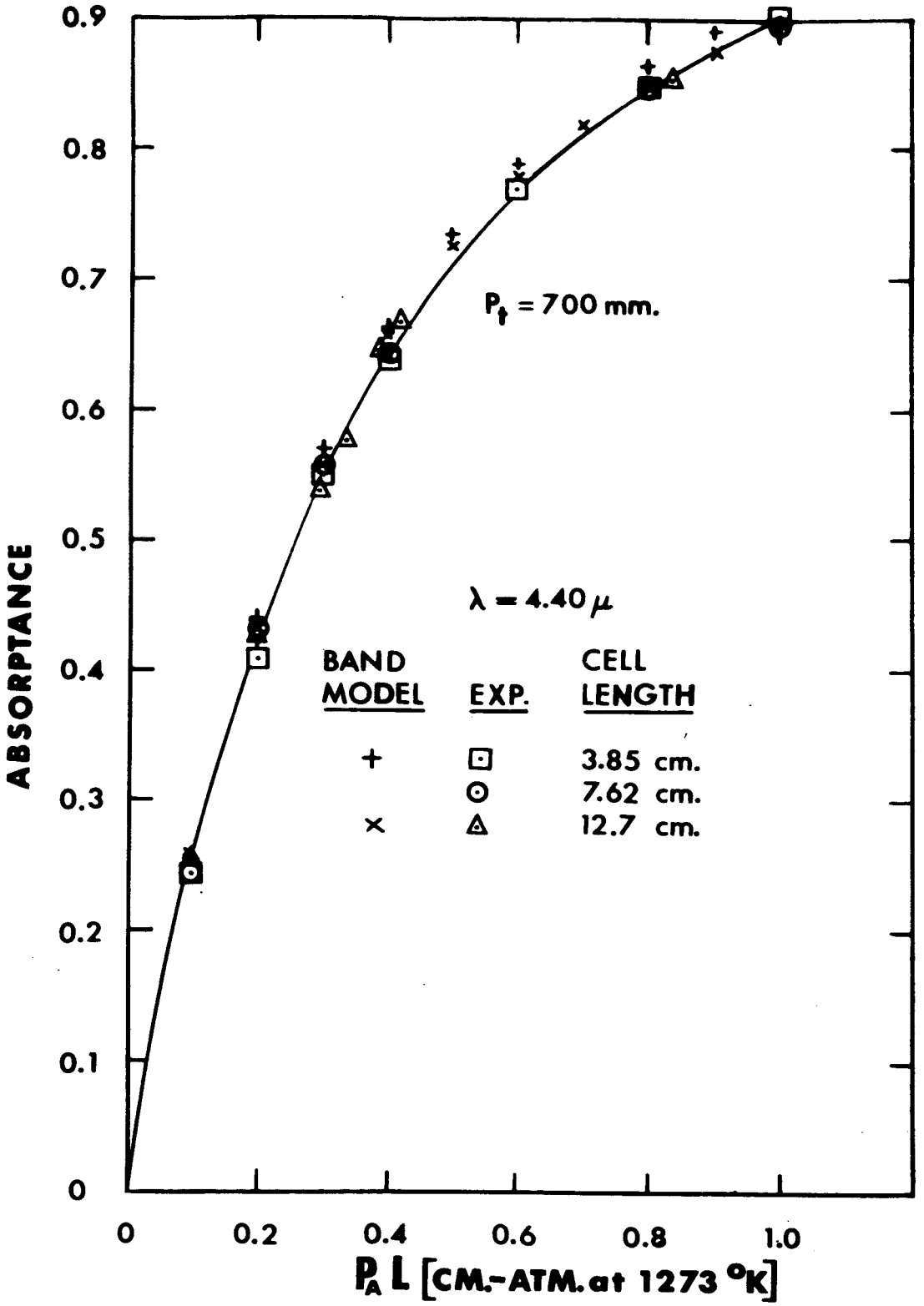

Fig. 6. Comparison of experimental data and band model prediction for CO_2-N_2 mixtures at 1273°K. The curve is the best fit of the experimental data.

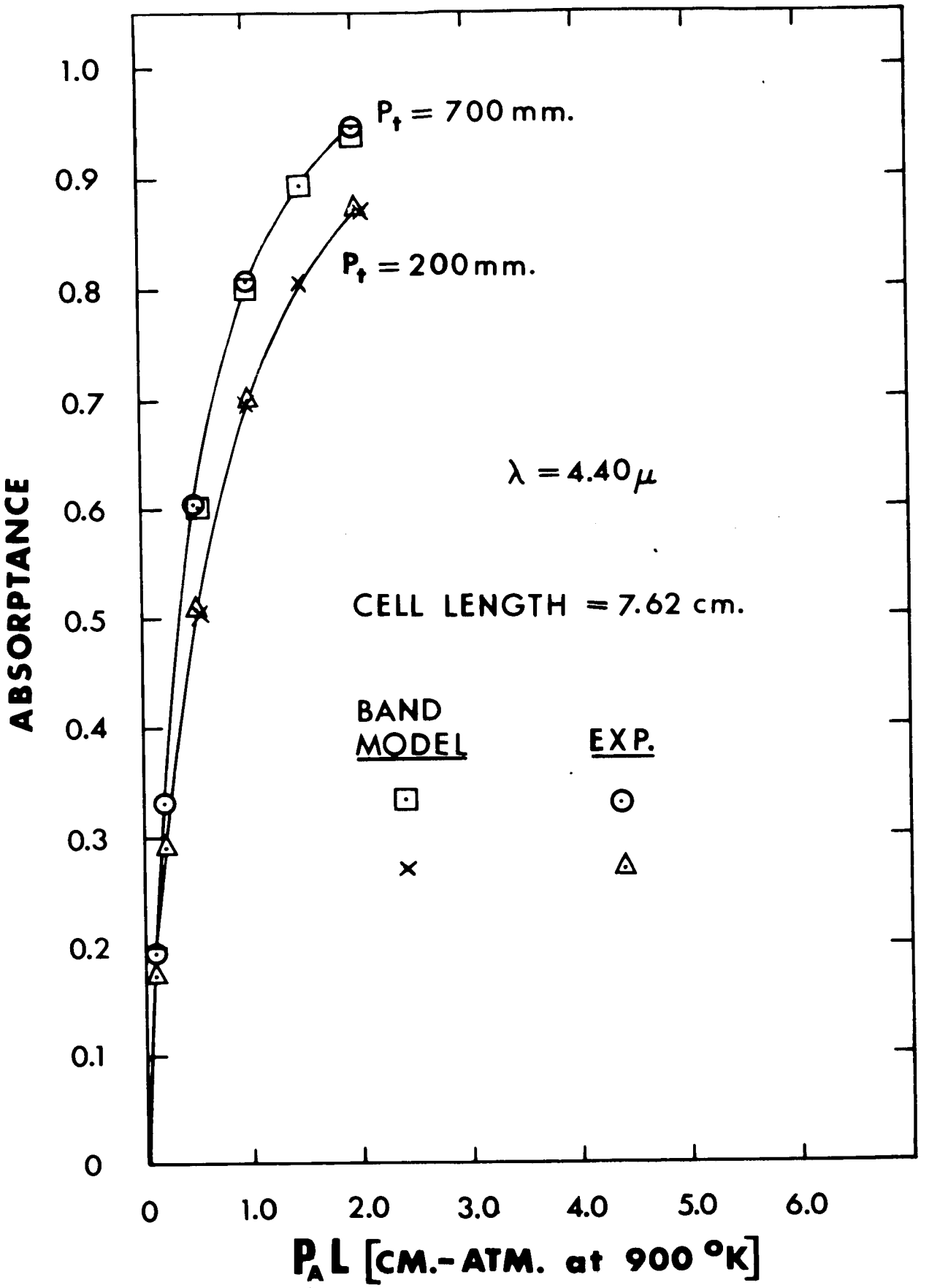

Fig. 7. Comparison of experimental data and band model temperature interpolation for CO_2-N_2 mixtures at 900°K. The curve is the vest fit of the experimental data.

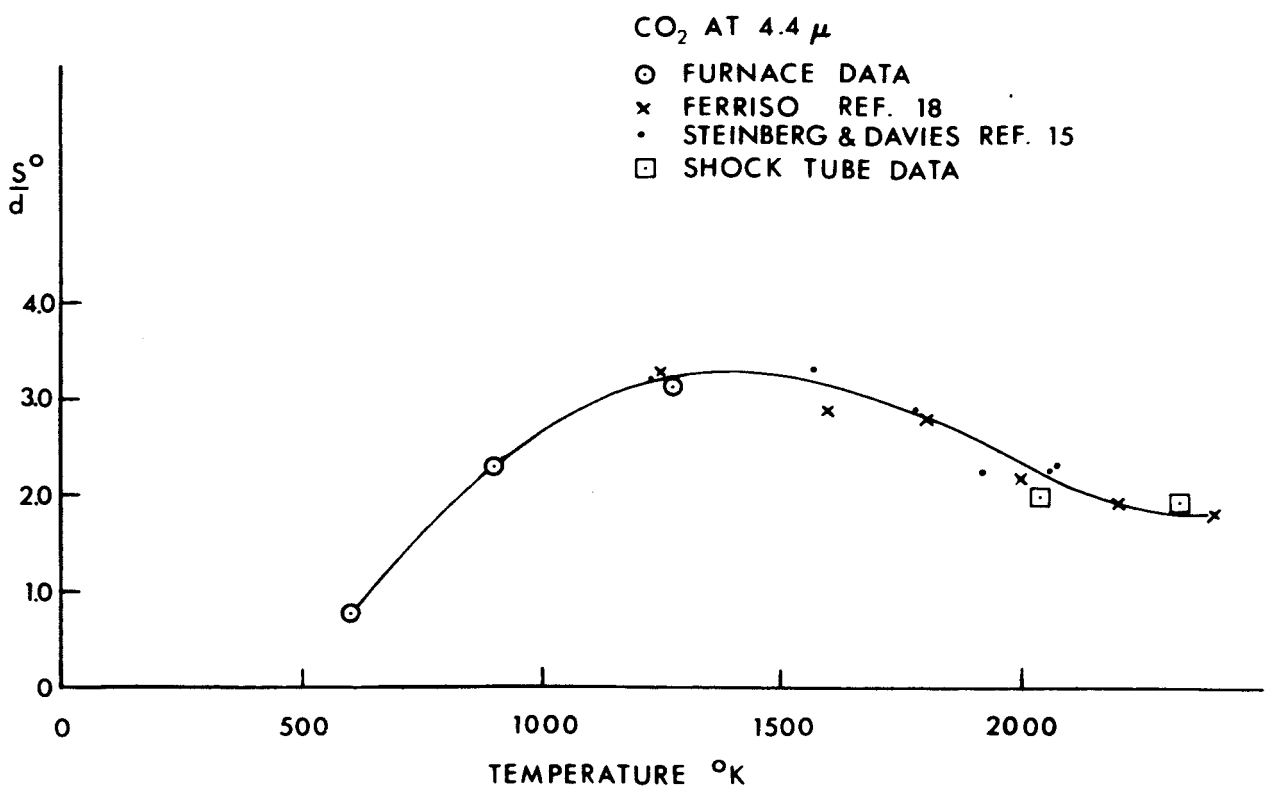

Fig. 8. Strength band model parameter $(S^\circ/d)_{CO_2}$ versus temperature.

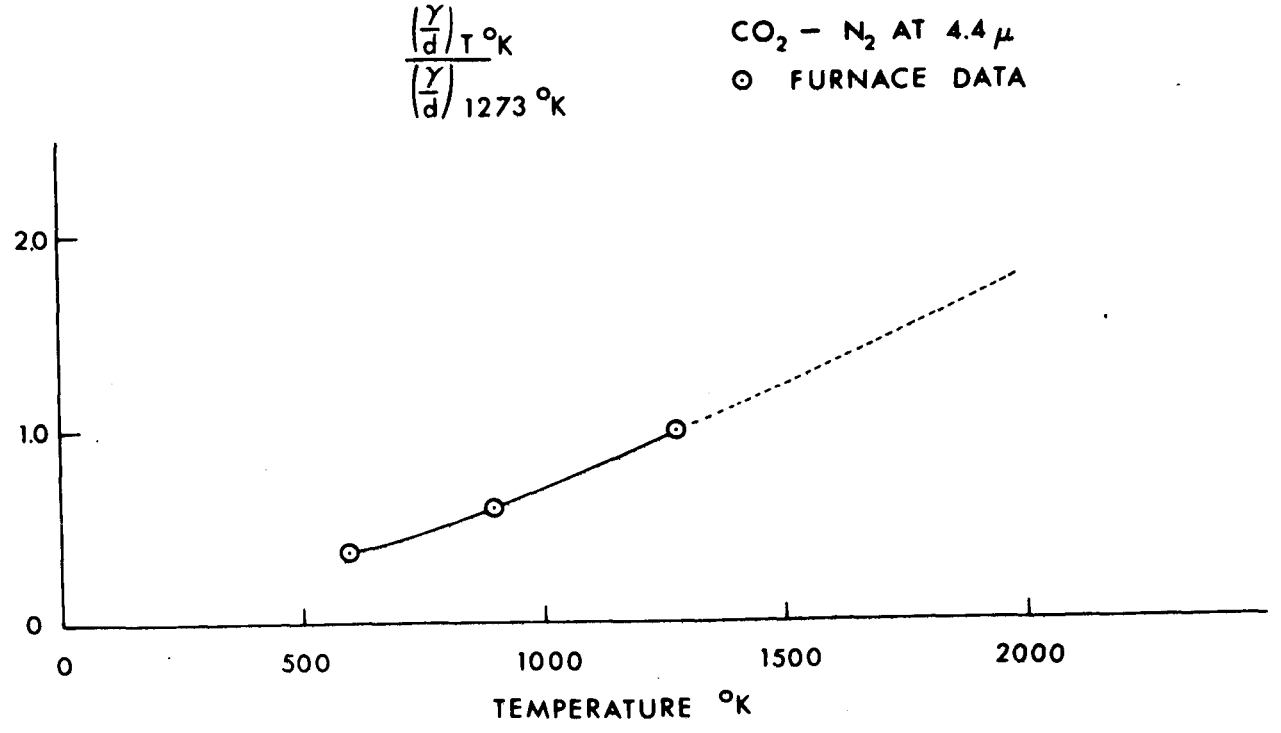

Fig. 9. Ratio of total half-width band model parameter $(\frac{\gamma^o}{d})_T$, to half-width $(\frac{\gamma^o}{d})_{1273}$ at 1273°K versus temperature.

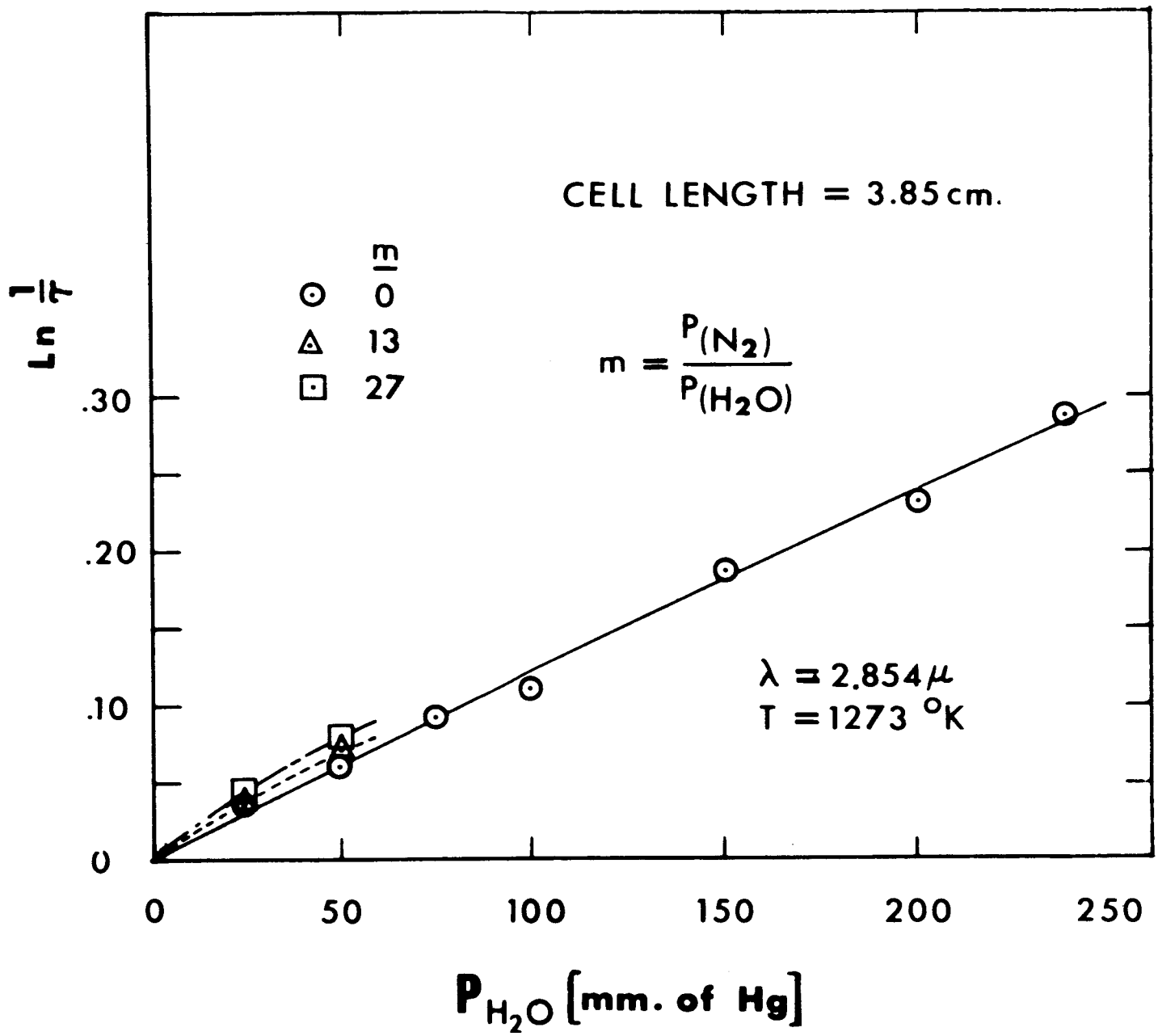

Fig. 10. H_2O absorption for several mixture ratios of H_2O and N_2 at 2.854-μ and 1273°K for 3.85 cm path length.

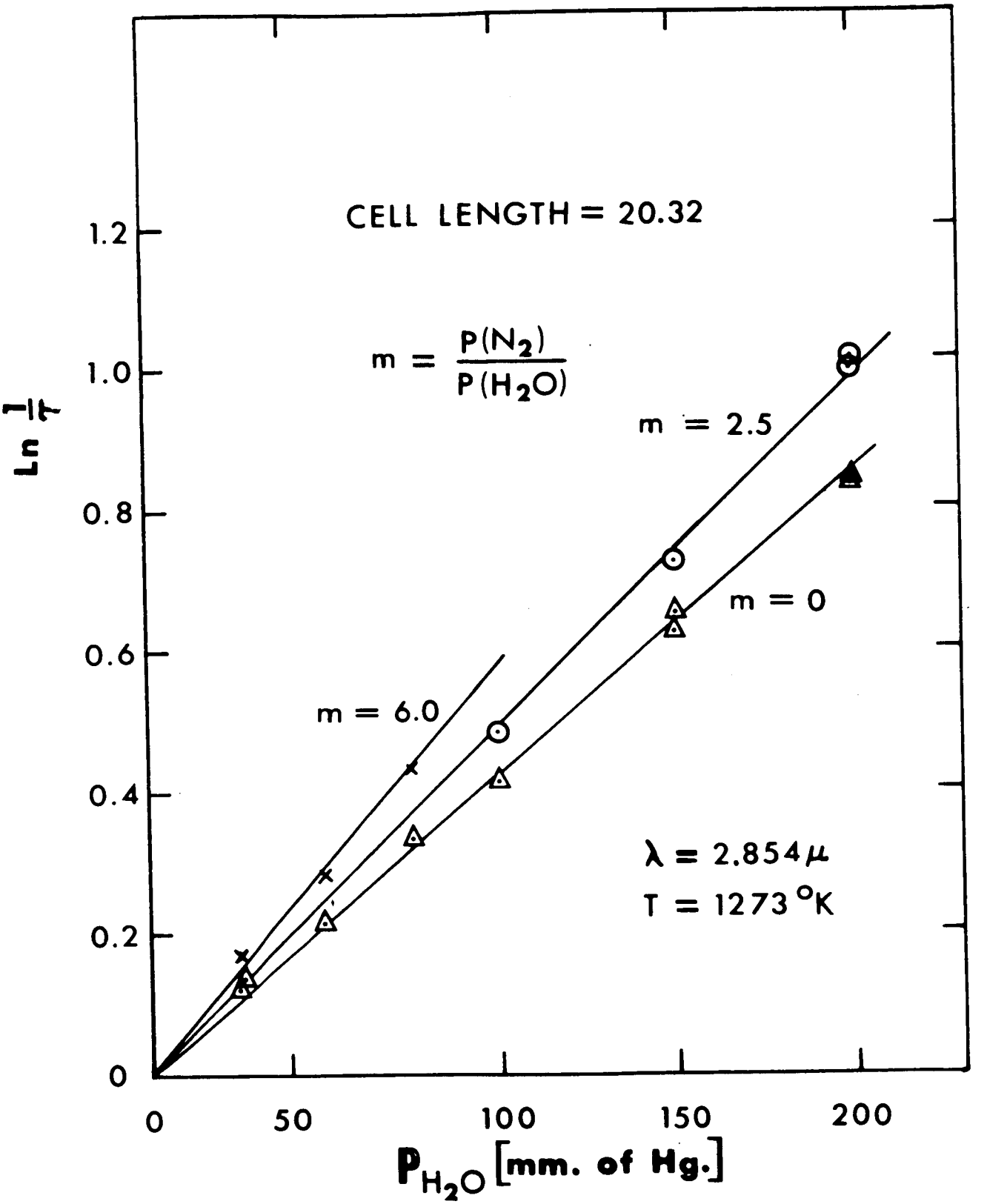

Fig. 11. H_2O absorption for several mixture ratios of H_2O and N_2 at 2.854-μ and 1273°K for a 20.32 cm path length.

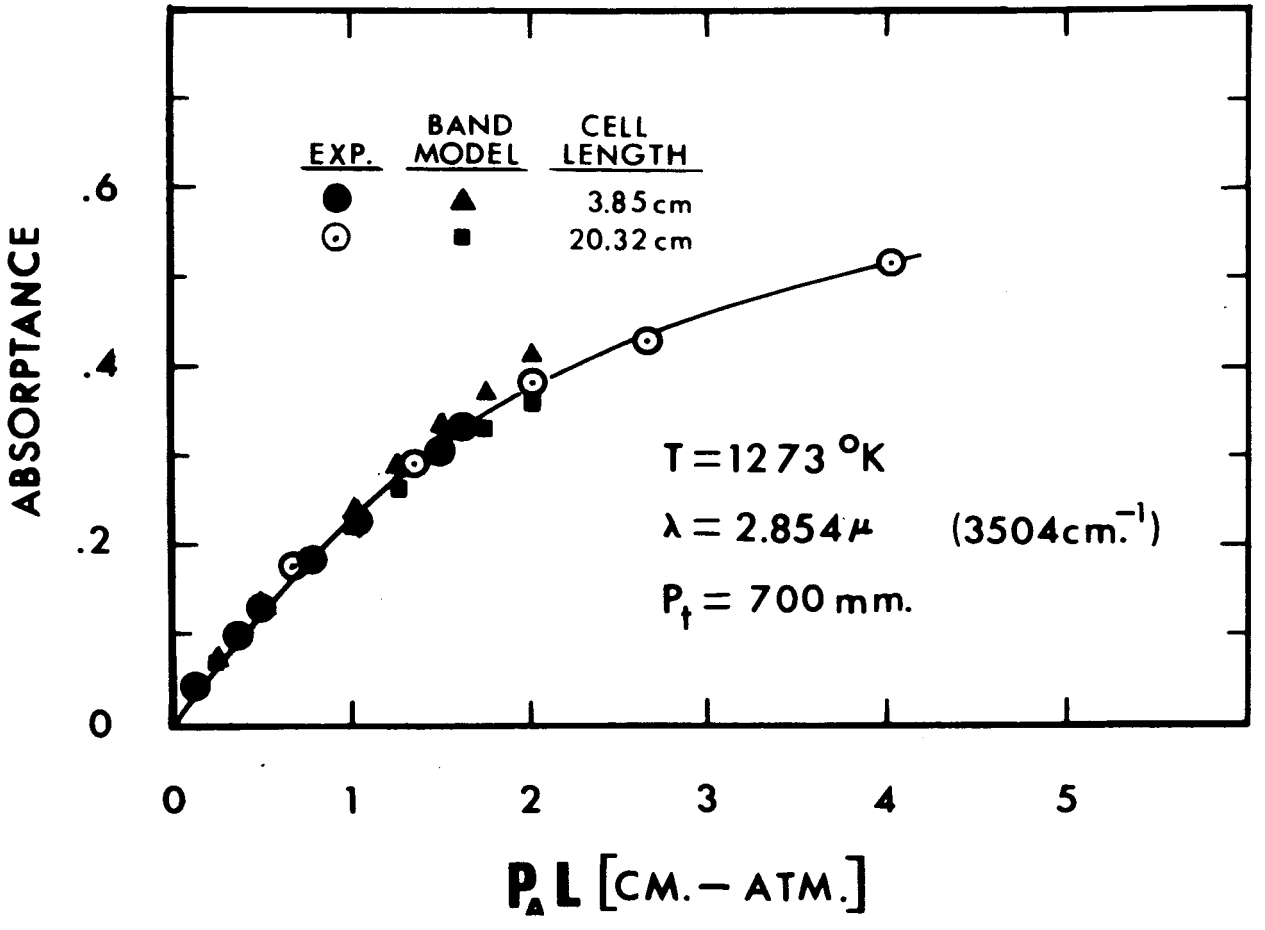

Fig. 12. Comparison of experimental data and band model prediction for H_2O-N_2 mixtures at 1273°K. The curve is the best fit of the experimental data.

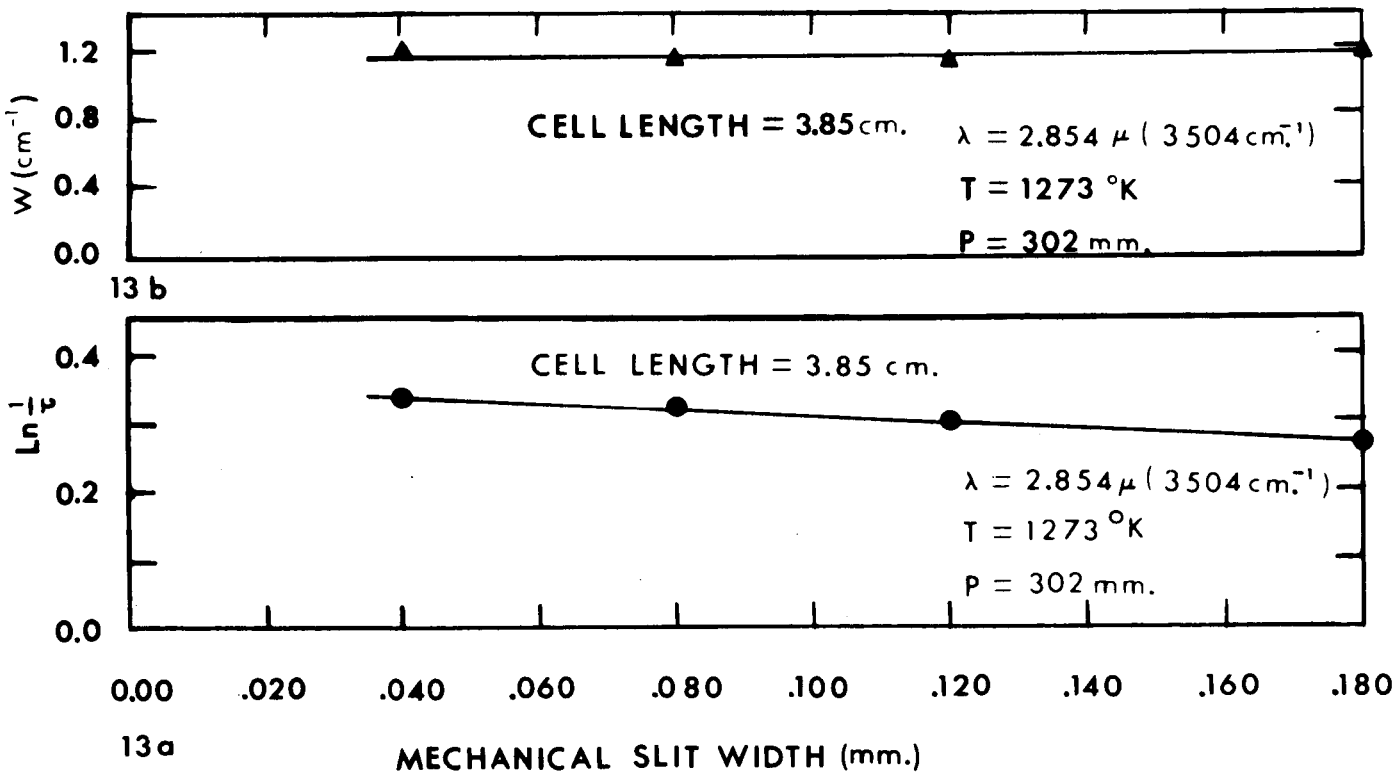

Fig. 13. Effect of spectral slitwidth on spectral absorptance and integrated absorptance (equivalent width) for pure H_2O. The lower curve (13a) is a plot of reciprocal transmittance vs the spectrometer slitwidth, for the peak of the spectral transmittance curve at 3504 cm^{-1}. The upper curve (13b) is a plot of equivalent width (area under the spectral transmittance curve, divided by I_o) of the same spectral interval. This example illustrates the well known fact that integrated absorptances are independent of spectral resolution.

DISTRIBUTION LIST

NASA Lewis Research Center
21000 Brookpark Road
Cleveland, Ohio 44135
Attn: E. A. Lezberg
MS 6-1

NASA Lewis Research Center
21000 Brookpark Road
Cleveland, Ohio 44135
Attn: W. S. DuCharme
MS 0-2

NASA Lewis Research Center
21000 Brookpark Road
Cleveland, Ohio 44135
Attn: Norman T. Musial

NASA Scientific and Technical
Information Facility
Box 5700
Bethesda, Maryland
Attn: NASA Representative

NASA Lewis Research Center
21000 Brookpark Road
Cleveland, Ohio 44135
Attn: Library

NASA Lewis Research Center
21000 Brookpark Road
Cleveland, Ohio 44135
Attn: Report Control Office

National Aeronautics and
Space Administration
Washington, D. C. 20546
Attn: Office of Advanced
Research and Technology,
Attn. H. H. Kurzweg,
Director of Research

NASA Lewis Research Center
21000 Brookpark Road
Cleveland, Ohio 44135
Attn: Henrikas V. Bankaitis
MS 0-5

National Aeronautics and
Space Administration
Washington, D. C. 20546
Attn: Office of Advanced
Research and Technology,
Attn. Nelson Rekos
Code RAP

National Aeronautics and
Space Administration
Washington, D. C. 20546
Attn: Office of Advanced
Research and Technology,
Attn. H. Burlage
Code RP

NASA Lewis Research Center
21000 Brookpark Road
Cleveland, Ohio 44135
Attn: Office of Reliability
and Quality Assurance

NASA Ames Research Center
Moffett Field, California 94035
Attn: Library

NASA Ames Research Center
Moffett Field, California 94035
Attn: Edward Perkins

NASA Flight Research Center
P. O. Box 273
Edwards, California 93523
Attn: Library

NASA Flight Research Center
P. O. Box 273
Edwards, California 93523
Attn: Jack Nugent

Jet Propulsion Laboratory
4800 Oak Grove Drive
Pasadena, California 91103
Attn: Library

NASA Langley Research Center
Langley Station
Hampton, Virginia 23365
Attn: Library

NASA Langley Research Center
Langley Station
Hampton, Virginia 23365
Attn: Dr. Kennedy Ruppert

Dr. Marvin C. Abrams
Staff Scientist
Physics & Infrared Section
General Dynamics/Pomona
Pomona, California

Dr. David Altman
United Technology Center
P. O. Box 358
Sunnyvale, California

Mr. R. Anschutz
Pratt & Whitney Aircraft
Florida Research & Devel. Center
Division of United Aircraft Corp.
P. O. Box 2691
West Palm Beach, Florida

Dr. James Balance
NASA Marshall Space Flight Center
Thermal Environment Laboratory
Huntsville, Alabama

Dr. Stanley Ballard
Physics Department
University of Florida
Gainesville, Florida

Mr. David Barraclough
Associated Electrical Industries
(Manchester) Ltd.
Trafford Park
Manchester 17, England

Mr. John Barton
Sylvania Electronic Defense Laboratory
P. O. Box 205
Mountain View, California

Dr. A. M. Bass
3.06 220 Stu
National Bureau of Standards
Connecticut Ave. at Van Ness
Washington, D. C.

Professor S. H. Bauer
Chemistry Dept.
Cornell University
Ithaca, New York

Dr. J. M. Beér
Pennsylvania State College
Dept. of Fuel Technology
College of Mineral Industry
State College, Pennsylvania

Dr. C. M. Beighley
Materials & Research Dept.
Aerojet Liquid Rocket Plant
P. O. Box 1947
Sacramento, California

Dr. Frank Belles
NASA Lewis Research Center
21000 Brookpark Road
Cleveland, Ohio 44135

Dr. Louis Block, CROO
Radiometry Laboratory
Air Force Cambridge Labs.
Office of Aerospace Research
L. G. Hanscom Field
Bedford, Massachusetts

Lt. John Blume, DGPL
Rocket Propulsion Laboratory
Edwards AFB
Edwards, California

Dr. J. Boulton
Instrumentation Dept.
Aerojet Liquid Rocket Plant
P. O. Box 1947
Sacramento, California

Mr. Leroy Brewer
Rocket Test Facility
ARO, Inc.
Arnold Station, Tennessee

Dr. Tony Briglio
Jet Propulsion Laboratory
California Inst. of Technology
4800 Oak Grove Drive
Pasadena, California 91103

Dr. Darrell E. Burch
Aeronutronic
Ford Road
Newport Beach, California

Dr. Ali Bulent Cambel
Director, Gas Dynamics Lab.
Northwestern University
Evanston, Illinois

Dr. Robert O'B. Carpenter
Geophysics Corp. of America
Bedford, Massachusetts

Dr. Tucker Carrington
National Bureau of Standards
Connecticut Ave. at Upton St.
Washington, D. C.

Dr. Neil Chatterton
Infrared Research Group
Eglin AFB
Valparaiso, Florida

Mr. John Chisholm
Pratt & Whitney Aircraft
Florida Res. & Devel. Center
P. O. Box 2691
West Palm Beach, Florida

Dr. Paul Davies
Imperial College of Science & Technology
E.I. DuPont Research Div.
Prince Consort Road
London, S. W. 7, England

Dr. W. O. Davies
Armour Research Foundation
Research Department
Illinois Inst. of Technology
10 West 35 Street
Chicago 16, Illinois

DDC (Defense Documentation Center)
Cameron Station
Alexandria, Virginia 22314

Dr. F. Dougherty
Dept. 5294, Plant #8
Allison Division
General Motors Corp.
Indianapolis, Indiana

Dr. R. H. Dow
Aerojet Liquid Rocket Plant
P. O. Box 1947
Sacramento, California

Mr. Larry Dreyer, DGFD
Rocket Propulsion Laboratory
Edwards AFB
Edwards, California

Dr. J. T. DuBois
Aeronautical Res. Laboratories
Office of Aerospace Research
United States Air Force
Wright-Patterson AFB, Ohio

Dr. H. W. Emmons
Dept. of Applied Science & Engineering
Harvard University
Cambridge, Massachusetts

Dr. Monroe V. Evans
Department of Chemistry
University of Wisconsin
Madison, Wisconsin

Mr. John W. Farnum
Aerojet General Corp.
Liquid Rocket Plant
Dept. 8771, Building 3308
Box 1947
Sacramento, California

Dr. Miko Fayon
American Cyanamid
1937 W. Main Street
Stamford, Connecticut

Dr. Carmine Ferriso
General Dynamics/Astronautics
Space Science Laboratory
Mail Zone 596-00
P. O. Box 166
San Diego 12, California

Lt. Col. Fitzpatrick
Rocket Propulsion Laboratory
Edwards AFB
Edwards, California

Mr. M. H. Friedman
Minnesota Mining & Mfg. Co.
St. Paul 19, Minnesota

Dr. John Garing
Infrared Physics Laboratory/CROL
Air Force Cambridge Research Labs.
Office of Aerospace Research
L. G. Hanscom Field
Bedford, Massachusetts

Dr. A. G. Gaydon
Dept. of Chemical Engineering
Imperial College of Science & Technology
Prince Consort Road
London, S. W. 7, England

Mr. Robert Gelinas
RAND Corporation
1700 Main Street
Santa Monica, California

Dr. J. T. Gier
Institute of Engineering
University of California
Berkeley, California

Dr. S. A. Golden
Rocketdyne Division
North American Aviation
McGregor, Texas

Dr. Glenn Goodwin
NASA Ames Research Center
Moffett Field, California

Dr. Robert E. Gorton
Pratt & Whitney
Division of United Aircraft Corp.
East Hartford, Connecticut

Dr. David A. Grafton
E. H. Plesset Associates, Inc.
2444 Wilshire Blvd.
Santa Monica, California

Professor Jerry Grey
Dept. of Aeronautical Engineering
Princeton University
Princeton, New Jersey

Dr. Frank Harris
Aerospace Corporation
2400 El Segundo Blvd.
El Segundo, California

Dr. R. E. Henderson
Research Group
Allison Division
General Motors Corp.
Indianapolis, Indiana

Dr. W. F. Herget
Rocketdyne Division
North American Aviation,
6633 Canoga Avenue
Canoga Park, California

Dr. R. W. Hermsen
United Technology Corporation
P. O. Box 358
Sunnyvale, California

Dr. K. E. Hill
Applied Physics Laboratory
The Johns Hopkins University
Silver Spring, Maryland

Dr. Harold F. Hipsher
Propulsion Div. of the Office of Research & Technology
NASA
Washington 25, D. C.

Dr. Gordon Dugger
Applied Physics Laboratory
Johns Hopkins University
Silver Spring, Maryland

Dr. Oscar Holderer
NASA Marshall Space Flight Center
Huntsville, Alabama

Dr. H. C. Hottel
Mechanical Engineering Dept.
Massachusetts Inst. of Technology
Cambridge, Massachusetts

Dr. John N. Howard
Chief, Optical Physics Lab/CRO
Air Force Cambridge Research Labs.
L. G. Hanscom Field
Bedford, Massachusetts

Dr. Robert Huffaker
NASA Marshall Space Flight Center
Thermal Environment Laboratory
Huntsville, Alabama

Institute of Science & Technology
The University of Michigan
P. O. Box 618
Ann Arbor, Michigan
Attn: BAMIRAC Library

Dr. T. A. Jacobs
Aerospace Corporation
2400 El Segundo Blvd.
El Segundo, California

Dr. W. E. Kaskan
General Electric Company
Space Sciences Division
Missile & Space Vehicle Dept.
King of Prussia, Pennsylvania

Professor G. B. Kistiakowsky
Harvard University
Cambridge, Massachusetts

Mr. Sotiris Lambiris
Pratt & Whitney Aircraft
East Hartford, Conn.

Dr. B. Lewis
Combustion & Explosives Research
Union Trust Building
Pittsburgh, Pennsylvania

Dr. William Malkmus
General Dynamics/Astronautics
Space Science Laboratory
Mail Zone 596-20
P. O. Box 166
San Diego, California

Mr. W. K. McGregor, Jr.
Rocket Test Facility
ARO, Inc.
Arnold Station, Tennessee

Mr. L. H. Meuser, ASRNRS-34
Air Force Systems Command/RTD
Avionics Laboratory
Wright-Patterson AFB, Ohio

Dr. R. E. Meyerott
Lockheed Missiles & Space Co.
Research Laboratories
3251 Hanover Street
Palo Alto, California

Dr. Roger C. Millikan
General Electric Company
Research Laboratory
P. O. Box 1088
Schenectady, New York

Dr. Roger Moore
NASA Headquarters
Lunar & Planetary Exploration Branch
Fourth St. & Maryland Ave., S.W.
Washington, D. C. 25

Dr. Robert K. Morton
Department of Physics
Temple University
Philadelphia 22, Pennsylvania

Dr. Howard W. Neill
U.S. Naval Ordnance Laboratory
Corona, California

Dr. Noble Nerheim
Liquid Propellant Systems
Jet Propulsion Laboratory
California Inst. of Technology
4800 Oak Grove Drive
Pasadena, California 91103

Dr. D. B. Olfe
Dept. of Aeronautics
New York University
University Heights 53, N.Y.

Dr. W. T. Olson
Associate Director
NASA Lewis Research Center
21000 Brookpark Road
Cleveland, Ohio 44135

Professor A. K. Oppenheim
University of California
Berkeley 4, California

Dr. U. P. Oppenheim
Department of Physics
Israel Inst. of Technology
Haifa, Israel

Dr. Sidney Passman
RAND Corporation
1700 Main Street
Santa Monida, California

Dr. Alvin M. Payne
Measurement & Instrumentation Branch
NASA Marshall Space Flight Center
Huntsville, Alabama

Dr. S. S. Penner
Institute for Defense Analyses
1825 Connecticut Avenue
Washington 9, D. C.

Dr. Gilbert N. Plass
Southwestern Research Institute
Dallas, Texas

Dr. E. K. Plyler
Head, Physics Department
Florida State University
Tallahassee, Florida 32306

Dr. John C. Polanyi
Department of Chemistry
University of Toronto
Toronto 5, Canada

Mr. Pontious
Picatinny Arsenal
Technical Services Lab.,
ORDBB-DT3
Dover, New Jersey

Mr. L. A. Povinelli
NASA Lewis Research Center
Chemistry & Energy Conversion
21000 Brookpark Road
Cleveland, Ohio 44135

Mr. Ed Price
Chief of Aerothermochemistry
USNOTS
China Lake, California

Dr. R. D. Rawcliffe
Aerospace Corporation
2400 E. El Segundo Blvd.
El Segundo, California

Dr. T. Riethof
General Electric Company
Valley Forge Space Technology Center
P. O. Box 8555
Philadelphia 1, Pennsylvania

Dr. Milton Ritter
Aerospace Corporation
2400 E. El Segundo Blvd.
El Segundo, California

Mr. Donald M. Ross, DGGT
Rocket Propulsion Lab.
Edwards Air Force Base
Edwards, California

Dr. Theodore Rossman
Bell Aerosystems Company
P. O. Box 1
Mail Zone C-64
Buffalo 5, New York

Professor B. H. Sage
California Inst. of Technology
1201 E. California Street
Pasadena, California 91103

Dr. Karl Scheller, RRLC
Aerospace Research Laboratories
Office of Aerospace Research
United States Air Force
Wright-Patterson AFB, Ohio

Dr. Bertram Schurin
Geophysics Research Division
Air Force Cambridge Research Labs.
L. G. Hanscom Field
Bedford, Massachusetts

Dr. W. H. Sieber
NASA Marshall Space Flight Center
Huntsville, Alabama

Dr. Shirleigh Silverman
Office of Naval Research
Div. of Physical Sciences
Washington 25, D. C.

Mr. R. J. Sneeden
Curtiss-Wright Corporation
Woodridge, New Jersey

Dr. Irving Spiro
Aerospace Corporation
2400 E. El Segundo Blvd.
El Segundo, California

Dr. Martin Steinberg
Senior Physicist
General Motors Research
Goleta, California

Dr. Klaus G. P. Sulzmann
General Dynamics/Astronautics
Space Science Laboratory
San Diego 12, California

Dr. J. W. Sutton
Boeing Aircraft
Seattle, Washington

Dr. Russell Walker
Thermal Spectroscopy
Air Force Cambridge Research Labs.
L. G. Hanscom Field
Bedford, Massachusetts

Dr. Leland A. Watermeier
Chief, Combustion Section
Interior Ballistics Lab.,
Bldg. 390
Ballistic Research Labs.
Aberdeen Proving Grounds, Md.

Dr. Felix J. Weinberg
Imperial College of Science
& Technology
Prince Consort Road
London S.W. 7, England

Mr. Homer Wilson, Jr.
NASA Marshall Space Flight
Center
Aerodynamic Analysis Branch
Aeroballistics Division
Huntsville, Alabama

Mr. Arvel Witte
Liquid Propellant Systems
Jet Propulsion Laboratory
California Inst. of Technology
4800 Oak Grove Drive
Pasadena, California 91103

Dr. W. Wolfe
IRIA
Institute of Science &
Technology
University of Michigan
P. O. Box 618
Ann Arbor, Michigan

Dr. H. G. Wolfhard
Institute for Defense Analyses
1825 Connecticut Avenue
Washington 9, D. C.

Mr. Robert Ziem
Chief, Solid Propellant Branch
NASA Headquarters
Office of Advanced Research
& Technology
1520 H Street
Washington 25, D. C.

Dr. J. A. Sanderson
Naval Research Laboratory
(Code 2021)
Washington 25, D. C.

Mr. F. S. Simmons
Institute of Science & Technology
University of Michigan
P. O. Box 618
Ann Arbor, Michigan